The Cryosphere

Spatial and temporal variability of snow accumulation rate on the East Antarctic ice divide between Dome Fuji and EPICA DML

S. Fujita[1], P. Holmlund[2], I. Andersson[3], I. Brown[2], H. Enomoto[4,1], Y. Fujii[1], K. Fujita[5], K. Fukui[1,*], T. Furukawa[1], M. Hansson[2], K. Hara[6], Y. Hoshina[5], M. Igarashi[1], Y. Iizuka[7], S. Imura[1], S. Ingvander[2], T. Karlin[2], H. Motoyama[1], F. Nakazawa[1], H. Oerter[8], L. E. Sjöberg[3], S. Sugiyama[7], S. Surdyk[1], J. Ström[9], R. Uemura[10], and F. Wilhelms[8]

[1]National Institute of Polar Research, Research Organization of Information and Systems, Tokyo, Japan
[2]Department of Physical Geography and Quaternary Geology, Stockholm University, Stockholm, Sweden
[3]Division of Geodesy and Geoinformatics, The Royal Inst. of Technology, Stockholm, Sweden
[4]Kitami Institute of Technology, Kitami, Japan
[5]Graduate School of Environmental Studies, Nagoya University, Nagoya, Japan
[6]Department of Earth System Science, Faculty of Science, Fukuoka University, Fukuoka, Japan
[7]Institute of Low Temperature Science, Hokkaido University, Sapporo, Japan
[8]Alfred Wegener Institute for Polar and Marine Research, P.O. Box 120161, 27515, Bremerhaven, Germany
[9]Department of Applied Environmental Science, Stockholm University, Stockholm, Sweden
[10]Faculty of Science, Department of Chemistry, Biology, and Marine Science, University of the Ryukyus, Okinawa, Japan
*now at: Tateyama Caldera Sabo Museum, Toyama, Japan

Abstract. To better understand the spatio-temporal variability of the glaciological environment in Dronning Maud Land (DML), East Antarctica, a 2800-km-long Japanese-Swedish traverse was carried out. The route includes ice divides between two ice-coring sites at Dome Fuji and EPICA DML. We determined the surface mass balance (SMB) averaged over various time scales in the late Holocene based on studies of snow pits and firn cores, in addition to radar data. We find that the large-scale distribution of the SMB depends on the surface elevation and continentality, and that the SMB differs between the windward and leeward sides of ice divides for strong-wind events. We suggest that the SMB is highly influenced by interactions between the large-scale surface topography of ice divides and the wind field of strong-wind events that are often associated with high-precipitation events. Local variations in the SMB are governed by the local surface topography, which is influenced by the bedrock topography. In the eastern part of DML, the accumulation rate in the second half of the 20th century is found to be higher by ∼15 %

than averages over longer periods of 722 a or 7.9 ka before AD 2008. A similar increasing trend has been reported for many inland plateau sites in Antarctica with the exception of several sites on the leeward side of the ice divides.

1 Introduction

1.1 Surface mass balance of Antarctica

Sea-level rise has been a debated issue in recent climatological studies related to global warming (Lemke et al., 2007). One of the main uncertainties arises from the still unknown contribution of the Antarctic ice sheet (Alley et al., 2005). Hence, assessing the mass balance and surface mass balance (SMB) of the Antarctic ice sheet has been a major concern of recent studies (Arthern et al., 2006; Chen et al., 2006; Davis et al., 2005; Giovinetto and Zwally, 2000; Helsen et al., 2008; Van de Berg et al., 2006; Velicogna and Wahr, 2006). In addition, several approaches for constraining the mass balance of the Antarctic ice sheet are based on the interpolation of accumulation rates obtained from field data such as firn cores, snow pits or stake readings, sometimes using background

fields from satellite data to control the interpolation scheme (Arthern et al., 2006; Giovinetto and Zwally, 2000; Vaughan et al., 1999). However, large parts of the vast East Antarctic Plateau remain uncovered by the ground-based measurements needed for these continent-wide interpolations. Obtaining thorough data sets for the SMB of the East Antarctic Plateau has been a priority in this regard. In the period of the International Polar Year 2007–2009(IPY), several inland traverses were undertaken to achieve a range of scientific goals including determining the SMB (e.g., Anschütz et al., 2009; Holmlund and Fujita, 2009). A number of preliminary results have already been presented, in addition to those described in the present paper. An example of such efforts is the Norwegian-USA traverse (IPY) through East Antarctica. The traverse has provided new data sets for the SMB based on ground-based accumulation measurements through large parts of DML to the South Pole (Anschütz et al., 2009, 2011; Müller et al., 2010).

Another important concern related to the SMB is whether or not snowfall-driven growth of the East Antarctic ice sheet mitigates recent sea-level rises. Bromwich et al. (2004) used the mesoscale model MM5 as well as the so-called dynamic retrieval method (DRM) to study spatial and temporal variability of Antarctic precipitation. They also estimated the redistribution of snow due to snow drift using MM5 surface wind fields. Cullather et al. (1998) compared the spatial and temporal variability of net precipitation (precipitation minus sublimation) derived from European Centre for Medium-Range Weather Forecasts (ECMWF) operational analysis data with a variety of glaciological and meteorological observations and data sets. Glaciological estimates of the Antarctic mass balance have been performed repeatedly; over the last four decades many such compilations (e.g., Arthern et al., 2006; Giovinetto and Zwally, 2000; Vaughan et al., 1999) have been presented, with continuously increasing amounts of data and using increasingly sophisticated methods. Although considerable differences in the results of regional investigations exist, most studies agree that there has been a slight increase in Antarctic precipitation/accumulation during the past few decades (Lemke et al., 2007). However, Monaghan et al. (2006) derived a 50-year time series of snowfall accumulation over the Antarctic continent by combining model simulations and primarily ice-core observations. They found that there has been no significant change in snowfall since the 1950s, which indicated that Antarctic precipitation is not mitigating global sea level rise as expected. A study using a stretched-grid atmospheric general circulation model (GCM) by Krinner et al. (2007) yielded results predicting an increase of 32 mm w.e. yr^{-1} in the Antarctic mass balance until the end of the 21st century, which represents an increase of about 21 %.

1.2 Earlier studies of regional SMB

Many regional investigations have identified an increase in accumulation rate during the second half of the 20th century. In DML, ice cores covering a time span of ∼1000 yr have indicated temporal variations of the accumulation rate. Oerter et al. (2000) reported that accumulation rates decreased in the 19th century and increased in the 20th century in Amundsenisen, covering a 10° W-10° E sector of DML. Hofstede et al. (2004) demonstrated that the mean increase in the SMB in DML during the early 20th century was the largest within the past 1000 yr. A recent study by Igarashi et al. (2011) produced a time series of accumulation rates at Dome Fuji over the last 740 yr, and showed a remarkable resemblance to the data presented by Oerter et al. (2000) and Hofstede et al. (2004) near the EPICA DML site. A compilation of the 37-yr history of the SMB at the South Pole (Mosley-Thompson et al., 1999) suggested an increase in the annual accumulation rate since 1965. At Dome C, Frezzotti et al. (2005) found a recent accumulation rate increase to 32 $kg^{-2} a^{-1}$, which can be compared to the long-term mean of 25.3 $kg^{-2} a^{-1}$ (1815–1998). They also reported a general increase in the accumulation rate at several drill sites along the transect from Terra Nova Bay to Dome C. In their cores, the period 1966–1998 shows a 14 to 55 % higher accumulation rate than the period 1815–1998. Stenni et al. (2002) found that the accumulation rate at Talos Dome had increased by 11 % during the 20th century in comparison to the 800 yr mean. However, Frezzotti et al. (2007) reported no significant increase in the accumulation rate over the last two centuries near Talos Dome. Yet Urbini et al. (2008) found significantly lower accumulation rates in the southwest of Talos Dome during the period 1835–1920 when compared with the period 1920–2001.

However, contrasting results have also been presented. Karlöf et al. (2005) investigated accumulation rates around "site M" (75.0° S, 15.0° E, see Fig. 1) in DML using firn cores and pit studies. They reported that the accumulation rate in the area has been stable over the last 200 yr. Isaksson et al. (1996) observed an accumulation rate decrease over the period 1932–1991 from a coastal core in DML and reported no change in accumulation rate for the period 1865–1991, based on another core from the plateau (75° S, 2° E, 2900 m a.s.l.). In addition, Isaksson et al. (1999) found that a general increase in accumulation rate, particularly in the latter part of the 20th century, was not necessarily the case for the whole polar plateau of DML. More recently, Anschütz et al. (2011) presented results from the Norwegian-USA scientific traverse. They reported that the largest changes seem to have occurred in the most recent decades with accumulation rates over the period 1963–2007/08 being up to 25 % different from the long-term record. They reported that there was no clear overall trend; some sites showed an increase in accumulation rate over the period 1963 to present while others showed a decrease. The data from almost all sites that are 3200 m or more above sea level suggested a decrease
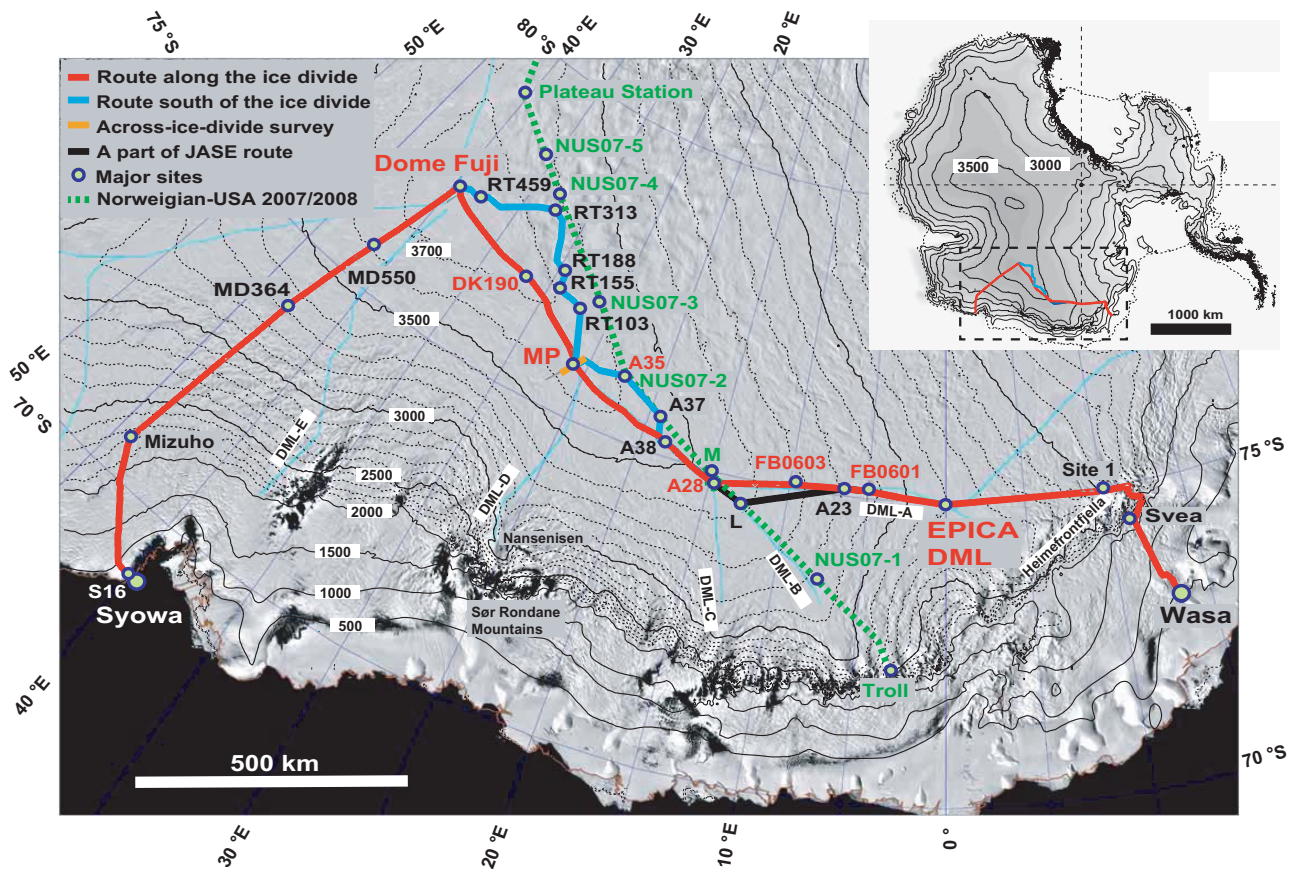
Fig. 1. Routes of the JASE traverse shown on a map of Antarctica. Surface elevation contour lines have a spacing of 500 m below 2000 m and of 100 m above 2000 m. The underlying satellite image is the MODIS mosaic of Antarctica (Haran et al., 2005). The red trace shows the route between S16 and Wasa. The blue trace shows the south routes (see text). Major sites are indicated by circular symbols (see also Table 1). Sites for pit studies and firn core studies are indicated by red letters. The orange line at MP is the trace of the cross-ice divide survey (see text). The black thick trace is also a part of the JASE traverse. The green dotted trace is the route of the Norwegian-USA traverse in the same 2007/2008 season (Anschütz et al., 2011). Site names related to it are indicated with green letters. Light blue thin traces indicate ice divides on the ice sheet surface. For convenience, we labelled the ice divides DML-A to DML-E.

in accumulation rate. Clearly, there are sites that showed no particular trend at all, and we note that many of these sites are located along the legs from Troll Station toward Plateau Station through site M, that is, along the route of the Norwegian-USA traverse.

1.3 Processes related to SMB

To form a better understanding of the SMB, we need to improve our knowledge on processes related to it, that is, the components that affect it, and their nature, character and amount. Until recently, it has always been assumed that precipitation on the Antarctic Plateau is almost entirely in the form of diamond dust, which is produced by in situ nucleation of ice crystals in extremely cold air without any synoptic dynamical forcing (e.g., Bromwich, 1988; King and Turner, 1997; Roe, 2005). However, both recent observa-

tions (e.g., Reijmer and Van den Broeke, 2003; Fujita and Abe, 2006) and model studies (e.g., Noone and Simmonds, 1998; Noone et al., 1999; Braaten, 2000; Schlosser et al., 2008) have shown that the interior plateau is influenced by the synoptic conditions in the coastal areas more strongly than previously thought. The investigations indicated above commonly show that several precipitation events occur per year that are responsible for a large part (more than 50 %) of the total annual precipitation on the inland plateau sites of DML, based on automatic weather station (AWS) observations, overwintering observations and/or model investigations. Reijmer and Van den Broeke (2003), for example, indicated that several precipitation events occur per year that can bring more than 50 % of the total annual precipitation near EPICA DML. Fujita and Abe (2006) created a data set of daily precipitation measurements at Dome Fuji for the year 2003. They observed precipitation almost daily, with

Table 1. Major sites along the JASE traverse and related sites.

Site name	Lat. ° S	Long. ° [a]	Elevation(m)	H (m)[b]	Note
S16	69.030	40.052	589	350	Base of the Japanese team near the coast.
Mizuho	70.697	44.274	2250	2060	
MD364	74.008	42.996	3347	2716	Mid-point between Mizuho and Dome Fuji
MD550	75.676	41.539	3663	2472	
DF	77.317	39.703	3800	3028	Dome Fuji Station: deep ice coring site (Watanabe et al., 2003)
DK190	76.794	31.900	3741	2919	Science stop for installing an automatic weather station
MP	75.888	25.834	3661	2820	Meeting point of the two teams. AWS JASE2007 was installed.
A38	75.287	18.421	3543	2706	Junction of the Swedish inbound and return trips
A28	74.862	14.742	3466	–	Junction of the Swedish inbound and return trips
RT459	77.376	37.932	3780	3333	Subglacial Lake Point
RT313	77.961	32.624	3620	3550	Southernmost point of the JASE traverse.
RT188	77.161	29.426	3678	2574	
RT155	76.869	29.270	3701	2702	
RT103	76.762	27.248	3653	3019	
A35	76.066	22.459	3586	–	One of the junctions between the JASE traverse and the Norwegian-USA traverse
A37	75.654	19.240	3544	–	Same as above
FB0603	75.117	9.724	3300	–	Firn coring site by the Alfred Wegener Institute, Germany in 2006
A23	75.168	6.493	3174	–	Junction of the Swedish inbound and outbound trips
FB0601	75.247	4.844	3090	–	Firn coring site by the Alfred Wegener Institute, Germany in 2006
EPICA DML	75.002	0.068	2890	2774	2774-m long ice coring site (EPICA Community Members, 2006)
Wasa Station	73.053	–13.374	292	383	Base of the Swedish team
Svea Station	74.571	–11.170	1313	715	Swedish station
IPY Site1	75.001	–10.121	2528	1603	Science site
Site M	75.000	15.000	3457	–	Science sites in Hofstede et al. (2004) and Isaksson et al. (1996)
Site L	74.647	12.790	3420	–	Junction with the Norwegian-USA traverse
NUS07-1	73.717	7.983	3174	–	Science sites in Anschütz et al. (2009, 2011) and Müller et al. (2010)
NUS07-2	76.067	22.467	3582	–	Same as above. Location is close to A35 within 300 m.
NUS07-3	77.000	26.050	3589	–	Same as above
NUS07-4	78.217	32.850	3595	–	Same as above
NUS07-5	78.650	35.633	3619	–	Same as above

[a] Positive and negative longitude number mean East and West, respectively.
[b] H: ice thickness (m).

only 18 days of non-diamond-dust precipitation during an observation period of 349 days. They found that half of the annual precipitation was accumulated episodically by only 11 events during these 18 days. Noone et al. (1999) carried out a comprehensive study of DML precipitation using ECMWF re-analysis data. They also found that a few synoptically induced precipitation events per year can yield a large part of the total annual accumulation. More recently, Schlosser et al. (2010) investigated high-precipitation events at EPICA DML, during the period 2001–2006 using Antarctic Mesoscale Prediction System (AMPS) archive data. The

precipitation was found to be highly episodic, with, on average, approximately eight high-precipitation events per year that are responsible for more than half of the amount of the total annual accumulation. The duration of the events varied from 1 day to about 1 week. On most the remaining days in the year, however, the daily precipitation was about one order of magnitude lower than that for the high-precipitation events. The synoptic weather patterns causing these events were directly associated with frontal cyclones systems in only 20 % of the 51 cases investigated. The majority of the events occurred in association with (blocking) anticyclones

and correspondingly amplified Rossby waves, which lead to advection of warm, moist air from relatively low latitudes. Therefore, these high-precipitation events appear to be one of the keys for better understanding the SMB. In an earlier study, the precipitation regime of DML was investigated by Schlosser et al. (2008) using AMPS archive data. They investigated the temporal and spatial distribution of precipitation and compared the results to a mass balance map produced from glaciological data of western DML by Rotschky et al. (2007). Schlosser et al. (2008) suggested that the mass balance map and the AMPS mean annual precipitation field showed similar patterns, which are mostly related to topography and prevailing wind systems. Precipitation is found to generally decrease from the coast to the inland plateau. Along the escarpment between the low-altitude coastal areas and the interior plateau, local minima and maxima in precipitation correspond to the leeward and windward sides of topographical ridges.

It has been recognized that precipitation has a major influence on the SMB, and that sublimation and redistribution of snow by wind can create large differences between precipitation and mass balance. Sublimation can amount to up to about 40 % of precipitation, especially in coastal areas (Bromwich et al., 2004). Frezzotti et al. (2004) suggested that wind-driven sublimation processes, controlled by the surface slope in the wind direction, have a huge impact (up to 85 % of snow precipitation) on the SMB. Redistribution of snow after a snowfall is also an important factor in mass balance estimates, since it can mean either positive or negative contributions to the mass balance of a given area. Therefore, the role of wind is also one of the keys to better understand the SMB. Earlier studies have shown that episodic precipitation events very often occur together with increases in wind speed and temperature (e.g., Birnbaum et al., 2010; Fujita and Abe, 2006; Schlosser et al., 2008, 2010). Birnbaum et al. (2010) showed in Fig. 6 of their paper a time series of daily precipitation rates from AMPS forecasts for 2002, together with periods identified as strong-wind events on the basis of the 2 hour mean values of wind speed measured at the AWS at EPICA DML. They stated that "not all strong-wind events are associated with high daily precipitation rates and vice versa". Nevertheless, their Fig. 6 shows that many strong-wind events are in fact associated with high daily precipitation. These earlier studies motivated us to search for a link between the SMB and strong-wind events.

1.4 JASE traverse

To better understand the spatio-temporal variability of the glaciological environment in DML, East Antarctica, a 2800-km-long traverse was carried out by the Japanese Swedish Antarctic Expedition (henceforth, JASE traverse) across DML in austral summer 2007/2008 (Holmlund and Fujita, 2009). The SMB was one of the main scientific goals and is discussed in the present paper in terms of spa-

tial distribution, temporal variation and related precipitation regimes/processes. The routes included two major ice-coring sites at Dome Fuji (Watanabe et al., 2003; Kawamura et al., 2010) and at EPICA DML (Oerter et al., 2004; EPICA Community Members, 2006), and the major ice divide as well as the branches of this ice divide between these two sites. For a correct climatic interpretation of deep ice cores, better understanding of the precipitation regimes/processes is very important. In addition, dome summits and ice divides are often chosen as sites for ice coring. Thus, these ice-coring sites were connected by the scientific traverse. The entire route covered areas in both the Antarctic Southern Atlantic Ocean sector and the Antarctic Indian Ocean sector, with a longitudinal coverage between ∼13° W and ∼42° E. We carried out thorough investigations of the ice-sheet environment including the SMB, surface elevation, surface slope, AWS-based wind field, surface snow reliefs, passive microwave remote sensing data and radar-based ice thickness. For the SMB investigation, we analyzed the age and water equivalent depth of isochrones based on data sets from snow pits, firn cores, and radars.

2 Traverse route and methods of investigation

2.1 Traverse route

Figure 1 shows a map of DML with the traverse routes indicated. The names of important sites on the map are listed in Table 1. The tracked-vehicle-based expedition used two starting points, the S16 site near the Japanese Syowa Station for the Japanese team and the Swedish Wasa Station for the Swedish team. The JASE traverse was along the trace connecting several Antarctic stations, Syowa-Dome Fuji-EPICA DML (Kohnen)-Wasa. The expedition began on 14 November 2007, for the Japanese team and on 5 December 2007, for the Swedish team, with a plan to meet at the meeting point (MP) on the polar plateau in late December, for joint scientific studies and exchange of crew members and scientific instruments such as radars, microwave radiometers and GPS receivers. Many of these scientific instruments were mounted on the vehicles, and were operated continuously along the traverse route. In addition, a new Argos-type AWS was installed at MP (Keller et al., 2010). The two teams met on 27 December at MP and began the return trip to their home stations, Syowa and Wasa, along routes partially different from the incoming ones (blue traces in Fig. 1) for both scientific and logistical reasons. The scientific reason was to investigate regions not only along the exact ice divides but also regions away from them. The logistical reason was that some of the fuel depots were located away from exact ice divides.

The JASE traverse route between S16 and Dome Fuji is located in the Shirase Glacier Drainage basin in the leg. We refer to this leg as the Dome Fuji route, which has been used since 1992 (e.g., Furukawa et al., 1996) for management of deep ice coring at Dome Fuji. In the leg between Dome Fuji
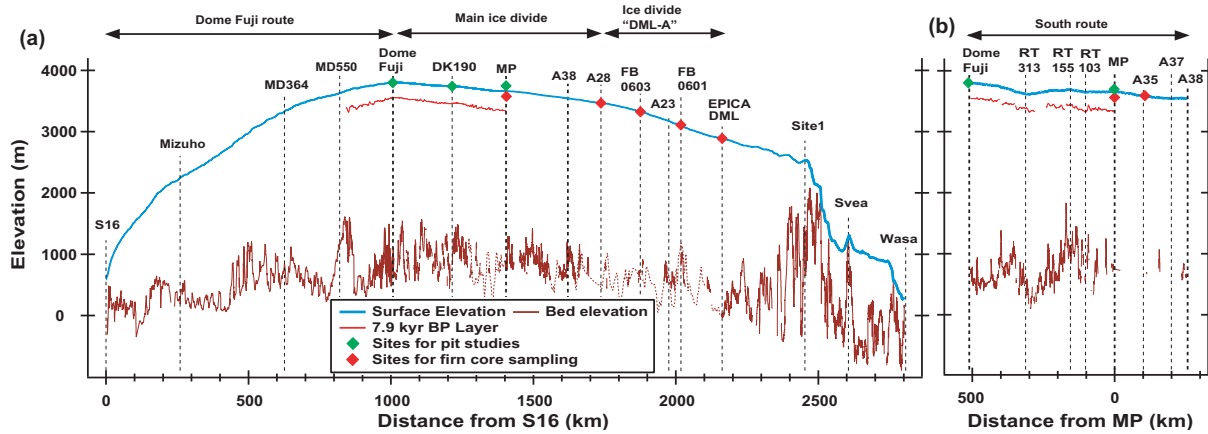
Fig. 2. Cross section of the ice sheet along the JASE traverse routes. **(a)** The main ice divide route (see red trace in Fig. 1). **(b)** The south routes (see blue traces in Fig. 1). Abscissas show **(a)** distance along the traverse from S16 toward Wasa Station and **(b)** distance from MP along the south routes. The vertical exaggeration is 200 times. Vertical dashed lines show the location of major sites. Surface elevation data (blue curves) are based on the digital elevation model of Bamber et al. (2006). A shallow isochrone within the ice sheet is shown as a red profile based on analysis of the radar sounding data. It is dated as the 7.9 ± 0.5 kyr BP layer (see text). Bed elevation was derived from the radar sounding data. For some locations where the bed signal was undetected in the JASE traverse, ice thickness data from an earlier airborne radar sounding (Huybrechts et al., 2009) is shown as a thin dotted profile. Sites with symbols indicate sites of pit studies and/or firn core sampling (see text).

and A28 (Fig. 1), the traverse is along the main ice divide. In the leg between the A28 site and EPICA DML, the traverse route runs along one of three branches of the ice divide originating at A28. For convenience, in the present paper, we label the ice divides DML-A to DML-E, as shown in Fig. 1. Among the three branches of the ice divides labeled DML-A, DML-B, and DML-C, DML-A is located at the southernmost, interior side of the Antarctic continent. Along the main ice divide, the wind direction for strong-wind events is between NE and ENE, as we will discuss later in this paper. Thus, the NNE and SSW sides of the main ice divide often represent the upwind and leeward sides, respectively, which influences the depositional environment. For convenience, we refer to the route between Dome Fuji and A28 along the ice divide as the "main ice divide route" in this paper. We refer to the blue trace in Fig. 1 as the "south route", which represents a depositional environment different from that of the main ice divide. The south route is located in the area between the main ice divide and the Norwegian-USA traverse 2007/2008 (green dashed trace in Fig. 1). Figure 2 shows a cross section of the ice sheet along the main ice divide route and the south route, which gives a large-scale view of surface and bedrock elevation along the traverses.

In addition to these long traverses, we created a survey route orthogonal to the ice divide from a point 60 km NNE of MP to a point 20 km SSW of MP. This was carried out to obtain information on the environmental gradient across the ice divide. In the present paper, we present data for a 40-km long section of this "cross-ice divide" survey centred on MP (orange trace in Fig. 1).

2.2 Methods of investigation of accumulation rate

Accumulation rate measurements were carried out using several ground-based methods such as snow pit studies, firn core studies and analysis of isochronous events in radar signals. This combination of methods, with supporting information from the two deep ice-coring sites, provided datasets for the accumulation rate along the traverse averaged over various time scales. We note that a review by Eisen et al. (2008) provides an overview of the various techniques used to measure the SMB as well as related difficulties and the limitations of data interpretation.

2.2.1 Snow pit studies

Two 4-m deep pits were dug at a site near Dome Fuji and at MP. In addition, a 2-m deep pit was dug at the DK190 site (Fig. 1 and Table 1). The pit near Dome Fuji was located at 77.298° S and 39.786° E, about 3 km from the station in the northeast direction, and was upwind of the prevailing wind direction to avoid possible chemical contamination from the station. Chemical constituents were analyzed with a depth resolution of 2 cm at the National Institute of Polar Research, Japan. By analysis of the major ions such as non-sea-salt sulphate (henceforth, nss-sulphate), we identified nss-sulphate peaks originating from the Agung (Indonesia) 1963 eruption (e.g., Pruett et al., 2004) and/or the Pinatubo (Philippines) 1991 eruption (e.g., Legrand and Wagenbach, 1999) in order to estimate the average accumulation rates since deposition of related aerosols in Antarctica.

The Agung eruption occurred in March 1963, and subsequent deposition of nss-sulphate in Antarctica began with a 6 month time lag (e.g., Göktas et al., 2002; Traufetter et al., 2004). Thus, we use the nss-sulphate peak for the Agung 1963 eruption as a time marker for the year 1964. Similarly, the deposit associated with the Pinatubo 1991 eruption occurred in 1992–1994 (Cole-Dai et al., 1997). The deposition of the Pinatubo sulphate aerosol was delayed due to the long transport route to high southern latitudes and its initial existence at high altitudes in the Antarctic atmosphere (Cole-Dai et al., 1997). Therefore, this was used as a time marker for the year 1993. Tritium peaks and physical stratification were also used to determine the depth/age relation. Snow density was measured from the wall of the pit with a depth resolution of 3 cm, which gave an estimate of the water equivalent depth. Water equivalent depths for the nss-sulphate peaks were used to derive accumulation rates averaged over 44 yr (1964–2007/2008) for the Agung 1963 eruption and over 15 yr (1993–2007/2008) for the Pinatubo 1991 eruption. We estimated that the major source of errors was the spatially inhomogeneous deposition (e.g., Kameda et al., 2008), which can affect the depth determination of a target layer as thick as one year's deposition. Naturally, errors for averages over 44 yr for the Agung 1963 eruption are much smaller than those for averages over 15 yr for the Pinatubo 1991 eruption.

2.2.2 Firn core studies

Firn cores with lengths of ∼10 m were sampled at the MP, A35 and A28 sites during the 2007/2008 season by the JASE traverse team (Figs. 1 and 2, and Table 1). In addition, data from 14-m-deep firn cores sampled at FB0603, FB0601 and EPICA DML (Figs. 1 and 2, and Table 1) in the 2004/2005 and 2005/2006 seasons by the Alfred Wegener Institute (AWI), Germany, were used in this study. For these firn cores, dielectric profiling measurements (DEP) (Moore et al., 1989; Wilhelms et al., 1998) were carried out at the AWI to derive depth profiles of the high-frequency-limit electrical conductivity and density with a depth resolution of 5 mm. For all 6 firn cores, the depth corresponding to the Agung 1963 eruption was determined from the electrical conductivity peak that is known to be correlated with the nss-sulphate concentration (e.g., Wilhelms, 2005). For some cores, the deeper signal associated with the Krakatau 1883/1884 eruption was used as a reference. For these firn cores, the Pinatubo 1991 signal was not used because the firn cores were too brittle in the shallowest few meters to maintain their shape for the DEP measurements. The accumulation rates as well as their errors were determined in a similar way to those in the pit studies. Water equivalent depths were first derived using the firn core density. These were then divided by the age of the sulphuric acid deposit produced following the eruption.

2.2.3 Radars

Three different types of radars were used for investigating the accumulation rate. Table 2 gives a summary of the major isochrones used in this study, the three types of radars, and their spatial coverages. For convenience, we refer to the three types of radars as (i) the Japanese GPR (ground penetrating radar), (ii) Swedish GPR and (iii) POL179 radar.

The Japanese GPR is a short pulse radar. It was used along the traverse routes between the S16 and MP sites. The antenna was suspended on the side of the tracked vehicle so that it was always around 20 cm above the snow surface. In this study, we analyzed a horizon dated as 1286±3 AD. It was selected from many isochronous features for preliminary analysis because it was one of the shallowest traceable layers that existed over long distances. The analytical procedure was as follows. First, a data set for the two-way travel time (TWT) of the electromagnetic waves was compiled. TWT to depth conversion was carried out using the depth-density relation determined at the Dome Fuji coring site (Watanabe et al., 1997). The wave velocity along the propagation path was determined using the empirical relation between density and wave velocity (Fujita et al., 2000; Kovacs et al., 1995). This procedure enabled us to determine the depth of an observed internal layer at the Dome Fuji coring site (Table 2). The corresponding age of the layer was then assigned based on dating of firn cores at Dome Fuji (Igarashi et al., 2011). Water equivalent depths for the layers were determined assuming the same density profile as that measured for the Dome Fuji ice core, which was further cross-checked by the density profile of the Dome Fuji pit obtained in the present study. Finally, the water equivalent depths were divided by the age of the isochrone to derive the annual accumulation rate. In reality, depth-density profiles should have local variations, which must be taken into account during calculation of the accumulation rate. However, we estimated that the error caused by the local variability of the depth-density relations in traces from the plateau near Dome Fuji is a few % at most. This estimation is based on comparison between the water equivalent depth profile at Dome Fuji and EPICA DML (Ruth et al., 2007). The difference was found to be at most ∼6 %, despite a difference in elevation of ∼900 m. In addition, many pits in the JASE traverse and surface snow measurements (Fujita et al., 2008) showed little local variability.

The Swedish GPR is a step frequency continuous wave radar that detects conditions at shallow (<74 m) depths. Again, for preliminary analysis, we selected a single layer from the many traceable layers at each location. A prominent internal layer at a depth of 7.09 m at MP was first selected. The average snow density from the MP firn core to this depth ($\sim$450 kg m^{-3}) was used to calculate the depth of the layer based on a wave propagation speed of $\sim 2.35 \times 10^8$ m s^{-1}. The layer was dated to 79.3 yr old by scaling (in water equivalent depth) the Agung 1963 eruption signal found at 4.6 m depth in the firn core to a depth of 7.09 m. This scaling

Table 2. A summary of the three major isochrones used in this study and the three types of radars.

Date of three major isochrones	1286 ± 3 AD	79.3 ± 3 yr old before 2008 AD	7.9 ± 0.5 kyr before 2008 AD
Depth at major sites	37.3 m at DF, 46.6 m at MP	7.9 m at MP	242 m at DF, 319 m at MP
Name of the radar used in this paper	Japanese GPR	Swedish GPR	POL179 radar
Type of radar	Short pulse radar	Step frequency continuous wave radar	Pulse modulated radar
Specifications, manufacturer/model and/or reference papers	Geophysical Survey Systems Inc. model GSSI SIR-3000 with 270-MHz antenna	Frequency: 0.1–3.0 GHz, Band width: 600 MHz, References: Hamran and Aarholt (1993); Hamran et al. (1995); Richardson et al. (1997)	Frequency: 179 MHz, Band width: 14 MHz, Pulse width: 60 ns, Manufacturer: Sankosha Inc. Japan, Model: SKI-05053
Resolution	0.4 m	0.19 m	1.76 m
Investigation depth	74 m	50 m	3500 m
Scan rate	5 Hz	0.5–2 Hz	1 Hz
Samples per trace	2048	201	6000
Spatial coverage	All legs between S16 and MP including both the main ice divide route and the south route	Legs from MP to Wasa	Legs between MD364 and MP including both the main ice divide route and the south route

procedure means that we cannot compare values of the accumulation rate before and after the Agung 1963 eruption. This 79.3 yr old layer was traced to a point at a longitude of 7.00° E which is close to the A23 site (Fig. 1 and Table 1). In the leg with a longitudinal coverage between 7.00° E and 2.10° E, the same 79.3 yr old layer was not traceable. Instead, a deeper layer dated tentatively to 95.5 yr was traced. Also, in the leg with a longitudinal coverage between 2.10° E and 0°, a shallower layer dated tentatively to 57 yr was traced. Dating of these layers was achieved by linear scaling of the first isochrone of the 79.3 yr old layer at MP. Because of the date scaling at MP, detailed discussion of the absolute values of the accumulation rate is not possible. Instead, we use the accumulation rate values of the firn cores and an earlier compilation of accumulation rate data (Rotschky et al., 2007) in the same DML region as references, and adjusted the accumulation rate values to these. Overall, we use the Swedish GPR data only for discussion of variability and not for absolute values or their temporal changes.

POL179 radar is a 179-MHz pulse-modulated radar to observe deeper into the interior of the ice sheet. It detects phase and polarization both along and across the track. A 60 ns pulse was used to detect internal layers, and a 500 ns pulse to measure the thickness of the ice sheet. This radar was operated continuously along the traverse route. Prominent and persistent internal layers were traced. We used a layer dated at 7.9 ± 0.5 kyr BP, based on the Dome Fuji ice core, for analysis of the accumulation rate. This layer is deeper than ~200 m, but it is the shallowest layer that was traceable

at most sites including Dome Fuji. For the pulse-modulated radar, the receiver was switched off during pulse transmission in order to protect it from direct transmission. The depth of this layer was 242 m at Dome Fuji and 319 m at MP. Though there were many older and deeper prominent internal layers, we analyzed only this shallow layer because the effect of vertical strain is more difficult to take into account in deeper parts of the ice sheet. The 7.9 ± 0.5 kyr BP layer is located at depths shallower than 10 % of the water equivalent total thickness. Thus, the effect of strain is just a few percent when determining the accumulation rates from the water equivalent depths of the layer. The analytical procedure was as follows. First, a data set for the TWT of the electromagnetic waves was created. The depth of the internal layer was accurately determined using a set of calibration data from a down-hole radar target experiment at Dome Fuji (S. Fujita et al., unpublished data, 1997). We used the TWT for a radar target (ice coring drill) placed at accurately known depths in the ice coring hole. In order to calibrate the TWT data, we used electrical conductivity profile data from the Dome Fuji Station ice core (Fujita et al., 2002a) to identify the depths of major reflection horizons within the ice sheet. The calibrated TWT allowed us to identify the depths of the reflecting horizons. The age of the layer was then determined using existing dating data for the Dome Fuji ice core (Parrenin et al., 2007). By dividing the water equivalent depth by the age and correcting for vertical strain, the average annual accumulation rate was derived. To correct for the effect of vertical strain on the water equivalent thickness, we used a thinning function

based on a 1-D ice flow model at Dome Fuji (Parrenin et al., 2007). The model was designed specifically for ice coring sites such as Dome Fuji and Dome C, and has the advantage of being highly tuneable using information from ice cores. Ruth et al. (2007) showed that a 1-D glaciological ice flow model cannot be employed to determine a realistic chronology at the EPICA DML coring site for an ice time scale of up to 10^5 yr, because of the complex history of ice flow and accumulation along the flow path upstream of EPICA DML. In the present case, our analysis is limited to the summit region between MD550 and MP (Figs. 1 and 2) and to the shallow 7.9 kyr BP layer. Because the horizontal ice flow velocity is very small ($<1\,\mathrm{m\,s^{-1}}$) (e.g., Motoyama et al., 1995; Huybrechts et al., 2009), we assume that a 1-D glaciological ice flow model is still practical as long as we are willing to accept a small additional uncertainty. For example, the ratios of the water equivalent depth for the 7.9 kyr BP layer to the entire thickness at Dome Fuji and MP were 6.4 % and 9.3 %, respectively. Considering the effect of vertical compression (Fig. 5 in Parrenin et al., 2007), we applied a 3.5 % correction for the entire leg to account for vertical strain. We estimate that the error related to this thinning correction is at most ± 1.0 %.

2.3 Methods of investigation of the wind field

The wind field along the JASE traverse routes was investigated in two ways. Strong winds over the Antarctic ice sheet engrave the snow surface resulting in various types of reliefs, whose orientations can be used as proxy data for the traces of strong wind events. Sastrugi are classified as erosional structures with sharp ridges. Large dunes with heights of more than about $20 \sim 30$ cm and with smooth surfaces are depositional structures produced by very strong winds in the presence of snowfall. For both of these structures, the long axis indicates the wind direction. Earlier data for Eastern DML and Enderby Land were compiled as a folio by Kikuchi (1997). Birnbaum et al. (2010) investigated strong-wind events and their influence on the formation of snow dunes at EPICA DML. They reported that the formation of snow dunes only occurred for wind speeds of $>10\,\mathrm{m\,s^{-1}}$ at a height of 2 m caused by a low-pressure system. In the discussion section of this paper, we will discuss how the orientation of surface reliefs is related to strong-wind events and high-precipitation events. In this study, the orientation of the surface reliefs was measured using GPS compasses and/or magnetic compasses. The measurements were typically carried out every 10 km. To maintain homogeneous data quality, the same observer performed the measurements over a distance as long as possible.

The wind conditions were further analyzed using meteorological data recorded by an AWS installed by the JASE traverse team at MP. This is the only AWS providing data for the inland plateau of DML between Dome Fuji and EPICA DML. The AWS was set up by the Antarctic Meteorologi-

cal Research Center and Automatic Weather Stations Project, Space Science and Engineering Center, University of Wisconsin, Madison. The station name "JASE2007" was allocated to MP (Keller et al., 2010). The JASE2007 AWS has been operational since January 2008, and the data are available online (http://amrc.ssec.wisc.edu/). The observational items are temperature, air pressure, wind speed and wind direction. From these, we used wind speed and wind direction to investigate the relation between them. In addition, earlier AWS data at Dome Fuji, at MD364 (Takahashi et al., 2004) and at EPICA DML (Birnbaum et al., 2010; Reijmer and Van den Broeke, 2003) were also used to investigate the relation between wind speed and direction.

2.4 Polarization ratio of satellite-based microwave emissivity data at 6.9 GHz

Previous studies have shown that the polarization ratio of the microwave brightness temperature is linked to snow layering (Surdyk and Fily, 1993, 1995). The passive microwave data used in the present study were obtained from the Advanced Microwave Scanning Radiometer for EOS (AMSR-E), which was developed by JAXA for use on board the EOS satellite that has been in operation since 2002. The AMSR-E sensor measures both vertical and horizontal polarizations at 6.9, 10.65, 18.7, 23.8, 36.5 and 89.0 GHz. For the data used in the present study, the incident angle was approximately 55° from the zenith. The spatial resolution varied from 43 km at 6.9 GHz to 3.5 km at 89.0 GHz. The monthly mean brightness-temperature data for June 2003 were used. The polarization ratio, PR, is defined as follows:

$$\mathrm{PR} = \frac{\mathrm{TB_v} - \mathrm{TB_h}}{\mathrm{TB_v} + \mathrm{TB_h}} \tag{1}$$

where $\mathrm{TB_v}$ and $\mathrm{TB_h}$ are the vertical and horizontal components of the brightness temperature, respectively. We refer to the polarization ratio at 6.9 GHz as PR6.9. Surdyk and Fily (1993, 1995) found that the PR at frequencies below 10 GHz is a good indicator of the amount of stratification in the snow cover: the higher the PR, the larger the number of strata per unit depth, which correlates with a lower accumulation rate. We also note that microwave brightness temperature has little (less than a few kelvin) seasonal variability at frequencies near 6.9 GHz (e.g., Surdyk, 2002). Thus, the spatial distribution of the PR6.9 from the monthly mean data for June 2003 represents data for a much longer time span.

2.5 Ice thickness and surface slope measurements

Ice thickness and surface slope data are used for analysis of the conditions that influence snow accumulation. In addition to the POL179 radar, two more pulse-modulated radars were used to observe ice thickness along the traverse. They are a 179-MHz pulse-modulated radar (henceforth, VHF179 radar) and a 60-MHz pulse modulated radar (henceforth,

VHF60 radar) (Fujita et al., 1999; Matsuoka et al., 2002). All three radars had a peak power of 1 kW and three-element Yagi antennae, and used 500 ns or 1000 ns pulses. The POL179 radar was used in the legs between S16 and MP, including both the main ice divide route and the south route (see Fig. 1). The VHF179 radar was used in the legs between Wasa and MP. The VHF60 radar was used between EPICA DML and Dome Fuji.

The surface slopes were determined using the digital elevation model (DEM) (Bamber et al., 2006) and are shown in Figs. 3b, 4b and 9c. The surface slope is known to strongly influence the spatial distribution of the accumulation rate at various locations on the polar plateau (e.g., the Syowa-South Pole traverse – Endo and Fujiwara, 1973, the Dome Fuji-Syowa route – Fujita et al., 2002b; Furukawa et al., 1996, the DML-South Pole traverse – Anschütz et al., 2009, 2011; Müller et al., 2010 and near Dome C and Talos Dome – Frezzotti et al., 2005, 2007) because the combination of the prevailing wind, the steepness of the slope and the local surface topography determines the depositional environment.

3 Results

3.1 Accumulation rate

Annual accumulation rates averaged over periods after the Agung 1963 eruption and the Pinatubo 1991 eruption are listed in Table 3a and 3b. They are also displayed as symbols in Figs. 3a and 4a, which show data along the main ice divide route and the south route, respectively. We note that the value at FB0603 is lower than the surrounding firn core data points by $\sim$10 kg m^{-2} or $\sim$20 %.

The blue traces in Figs. 3a and 4a show the annual accumulation rate determined using the Japanese GPR. They show values averaged over 722 yr (1286–2008) along the ice divide and the southern route. Several features can be identified in the data: (i) generally, the Dome Fuji area exhibits low values; (ii) along the main ice divide route, the annual accumulation rate values are smoother and larger than for the south route; (iii) there are large fluctuations of up to $\sim$20 % along the south route and along the Dome Fuji route close to MD550; (iv) values are generally lower along the south route than along the main ice divide route.

The green traces in Figs. 3a and 4a show the accumulation rates determined using the Swedish GPR. As described in Sect. 2.2.3, averaging was performed over a variable time span of 57–95.5 yr. At the MP site, the radar result is identical to the 44 a average because the Agung 1963 layer was used as a scaling reference for the dating procedure.

Figure 2a and b show the 7.9 ka BP layer and the elevation of the bed in the cross section of the ice sheet. Despite the large variation of ice thickness from $\sim$2500 to $\sim$3400 m in the plateau region, the 7.9 ka BP layer is much smoother than the bedrock elevation. The accumulation rates averaged over

7.9 ka were determined and are plotted in Figs. 3a and 4a. We find that the values and variability of the 7.9 ka average are very similar to those of the 722 a average, despite a difference in age span of more than 10 times.

We compare the accumulation rate data from the present study with data presented in earlier publications for the purpose of cross-checking. The full set of data used for comparison is listed in Table 3a. At Dome Fuji, using 36 bamboo stakes, Kameda et al. (2008) estimated the mean accumulation rate over the period from 1995 to 2006 as 27.3 ± 0.4 kg m^{-2} a^{-1}. Figure 7 in Kameda et al. (2008) shows this error, which is the standard error of the mean annual SMB for multi-year averages. This result is also plotted in Figs. 3a and 4a, and is close to the average accumulation rates after 1964 AD (the Agung 1963 eruption). Furthermore, Igarashi et al. (2011) estimated the average accumulation rates from AD 1888 to 1993, and from AD 1993 to 2001 to be 28.3 ± 0.4 and 29.5 ± 5.2 kg m^{-2} a^{-1}, respectively. These values are close to those obtained in the present study for the average accumulation rates after 1964 AD (the Agung 1963 eruption), after 1993 (the Pinatubo 1991 eruption), and the value for 1995–2006 from the bamboo stake measurements (Kameda et al., 2008). In this way, the new data from the JASE traverse are consistent with earlier studies at Dome Fuji on different time scales.

3.2 Wind field

Figure 5 shows the dominant orientation of surface snow reliefs between MD364 and Wasa. The orientations are plotted as short thin lines with different colours on the map. At some sites, two or more orientations were observed, in particular at sites between A28 and A23 along the ice divide DML-A. In the field, the most dominant orientation was determined first, with secondary or less dominant orientations recorded when necessary.

Figure 6a shows meteorological data from the JASE2007 AWS at MP for the year 2009. Wind speed is plotted versus wind direction at intervals of three hours. Wind speeds above 10 m s^{-1} were only observed in 6 % of cases, with an average wind direction of $70 \pm 24°$. Wind speeds between 5 and 10 m s^{-1} were observed in 36 % of cases, with an average wind direction of $76 \pm 35°$. About 58 % of wind speeds were less than 5 m s^{-1} with an average wind direction of $97 \pm 58°$. The average wind-vector direction was also calculated from the meteorological data and was found to be 82° by an yellow arrow in Fig. 5. Near MP, the dominant orientation of surface snow reliefs (Fig. 5) was $70 \pm 10°$, which is in agreement with the wind direction for strong-wind events ($>$10 m s^{-1}).

In addition to the meteorological data recorded at MP, we examined meteorological data from the Dome Fuji, MD364 and EPICA DML sites using the data source described in Sect. 2.3. Figure 6b shows data from the CMOS-type AWS at Dome Fuji for the period between 1994 and 2001. Figure 6c

Table 3a. Annual accumulation rates derived for Dome Fuji, DK190 and MP.

Period (AD)	Time span	Site name			Data source	Error
		Dome Fuji	DK190	MP		
1993–2008	15	25.6 ± 1.7 (kg m^{-2} a^{-1})	34.1 ± 2.3	41.9 ± 2.8	Pit studies (JASE 2007/08)[a]	b
1995–2006	11	27.3 ± 0.4	–	–	Snow stake farm (Kameda et al., 2008)	c
1994–2001	7	29.5 ± 4.2	–	–	Analysis of firn core (Igarashi et al., 2011)	b
1964–2008	44	28.8 ± 0.7	–	38.7 ± 0.9	Firn core and pit studies (JASE 2007/08)	b
1286–2008	722	24.5 ± 0.7	$28.\,7 \pm 0.9$	33.1 ± 1.0	Japanese GPR (JASE 2007/08)	d
1260–2001	741	25.5 ± 0.3	–	–	Analysis of firn core (Igarashi et al., 2011)	e
–2008	7.9 ± 0.5 k	25.0 ± 1.3	28.7 ± 1.5	33.9 ± 1.7	Radar (JASE 2007/08) and Dome Fuji core	d

[a] Pit is located at 77.298° S and 39.786° E, and is ~3 km from the Dome Fuji Station.
[b] Error range was assumed to be equivalent to 1 yr accumulation, with a confidence level of ~83 %.
[c] Error is the standard deviation of the mean, with a confidence level of ~68 %.
[d] Major source of error was assumed to be caused by 3 % of the density estimation within firn.
[e] Major source of error was assumed to be caused by 1 % of the density estimation within firn.

Table 3b. Annual accumulation rates derived from firn core studies at sites between A35 and EPICA DML.

Period(AD)	Time span	Site name				
		A35	A28	FB0603	FB0601	EPICA DML
1964–2008	44	39.2 ± 0.9	44.5 ± 1.0	38.0 ± 0.9	51.6 ± 1.2	73.1 ± 1.7

Data source is firn cores (JASE 2007/08, AWI 2003/04 and 05/06).
Error type is b.

shows data from the Argos-type AWS at MD364 for the period between 2001 and 2003. Table 4 shows a comparison between the dominant orientations of surface snow reliefs and the analyzed wind directions. The reliefs tend to be aligned with the wind direction for strong-wind events, rather than the average wind-vector direction.

3.3 Polarization ratio of satellite-based microwave emissivity data at 6.9 GHz

Figure 7 displays the PR6.9 distribution, and its most important features can be listed as follows.

i. In general, the NE region exhibits lower PR6.9 values than the SW region.

ii. In the area between Dome Fuji and MP, a steep PR6.9 gradient occurs across the ice divide, with the NE side of MP having particularly low PR6.9 values. This suggests a rapid change in the stratification across the ice divide at MP.

iii. The leg between A28 and EPICA DML and the SW side of A28 are within the high PR6.9 zone, which suggests a higher number of strata per unit depth, possibly linked to a lower accumulation rate.

iv. There are several ice divide branches (DML-A to DML-E,). The NE side of the ice divide branches have lower PR6.9, which suggests a smaller number of strata per unit depth, possibly linked to a higher accumulation rate. The leeward side of the ice divide branches have higher PR6.9, possibly linked to a lower accumulation rate.

v. The route of the Norwegian-USA traverse (Anschütz et al., 2011) is located almost entirely in a region with relatively high PR6.9 values, which should be taken into consideration when attempting to determine the SMB.

The insights provided by the PR6.9 map into the distribution of the accumulation rate in this area will be discussed in the Sect. 4.

4 Discussion

4.1 Spatial distribution of SMB at and around the ice divides

4.1.1 Large-scale trend based on ground-based data

The accumulation rate is basically dependent on the elevation, continentality and geographical location of the sites relative to the the ice divides in DML, which we will now demonstrate using data. The elevation dependence is shown in Fig. 8 both for the main ice divide route and for the south route. It can be seen that the accumulation rate is lower at

Table 3c. Annual accumulation rates at several sites of the Norwegian-USA (NUS) traverse (Anschütz et al., 2011) in the vicinity of the JASE traverse.

Period(AD)	Time span	Site name				
		NUS07-1	NUS07-2	NUS07-3	NUS07-4	NUS07-5
1963[a]–2008	45	55.9 ± 3.9	28.0 ± 2.0[b]	23.7 ± 1.7	17.5 ± 1.2	20.7 ± 1.4
1259–2008	749	–	33.3 ± 1.2	–	–	26.0 ± 0.9

[a] Anschütz et al. (2011) used 1963 as date of deposition for the Agung eruption. Thus the NUS accumulation rate data should be ∼2 % lower than the JASE data.
[b] Some doubt about peak identification.

Table 4. Comparison between orientation of surface snow features and wind field

Site	Orientation of surface snow features (this work)[a]	Average direction of wind vector calculated from meteorological data	Wind direction for strong-wind events	Station ID of AWS or data source	Year of the observational data	Reference
EPICA DML	45° (this work)	57°[b]	45°	Utrecht University/ IMAU AWS9	1998–2000, 2002–05	Birnbaum et al. (2010), Reijmer and Van den Broeke (2003)
MP	70°	82°	70 ±24°[c]	ARGOS AWS No. 30305 (JASE2007)	2009	Keller et al. (2010)
Dome Fuji	50°	100°	53 ±48°[d]	CMOS AWS at Dome Fuji Station	1994–2001	Takahashi et al. (2004)
MD364	102°	119°	120 ±22°[e]	ARGOS AWS No. 8198	2002	Keller et al. (2010)

[a] Mean value in the vicinity of each site, with errors of ±10°.
[b] Value at EPICA DML is cited from Birnbaum et al. (2010).
[c] An average wind direction for wind speeds above $10\,\mathrm{m\,s^{-1}}$ observed in ∼6 % of cases.
[d] An average wind direction for wind speeds above $8\,\mathrm{m\,s^{-1}}$ observed in ∼1 % of cases.
[e] An average wind direction for wind speeds above $10\,\mathrm{m\,s^{-1}}$ observed in ∼14 % of cases.

Table 5. Components of surface mass balance.

Surface accumulation or surface ablation	Sub components
Surface accumulation	Precipitation due to high-precipitation events[a]
	Precipitation due to diamond dust
	Deposition of hoar frost
	Deposition of drifted snow
Surface ablation	Sublimation
	Erosion due to snow drift

[a] Major (50–80 %) component of precipitation in polar plateau of DML.

higher elevation. Another important trend is that the accumulation rate is lower for the south route than for the main ice divide route. This situation can be clearly seen by comparing Figs. 3a and 4a. Also, in Fig. 8a, the data along the main ice divide and along the south route are clearly distributed at different levels. The data from the Norwegian-USA travese (Anschütz et al., 2011) are also listed in Table 3c for comparison. The values for sites NUS07-2 to NUS07-5 are almost as low as those for the south route, confirming the continentality trend. In addition, the data along the main ice divide is stable

and smooth (Figs. 3a and 8a) whereas that along the south route is subject to large fluctuations (Figs. 4a and 8a). The main ice divide and dome have singular features corresponding to unique ice sheet glaciological conditions (ice flow, surface topography etc.), so it seems quite natural that smoother SMB results would be found compared to the sloped ice sheet surface of the south traverse. Another large-scale trend is that along the ice divide branch between the A28 site and EPICA DML, the accumulation rate fluctuates. Such a pattern is also visible on the accumulation rate map compiled by Rotschky et al. (2004, 2007). We also note that in the leg between A28 and A23, the accumulation rate is lower than that obtained by a linear interpolation between the accumulation rates on the main ice divide route and near EPICA DML (see Figs. 3a and 8a).

The gradient of the accumulation rate versus distance along the main ice divide is $-0.02\,(\mathrm{kg\,m^{-2}\,a^{-1}})\,\mathrm{km^{-1}}$ (decreasing toward higher elevation) for the leg between Dome Fuji and MP in Fig. 3a. Also, the gradient of the accumulation rate versus elevation along the main ice divide is $-0.04\,(\mathrm{kg\,m^{-2}\,a^{-1}})\,\mathrm{m^{-1}}$ (decreasing toward higher elevation). To better understand the gradient of accumulation rate across the ice divide, data from the cross-ice divide survey at MP was analyzed. The accumulation rate along a 40-km leg is shown in Fig. 9a, together with information on surface elevation,
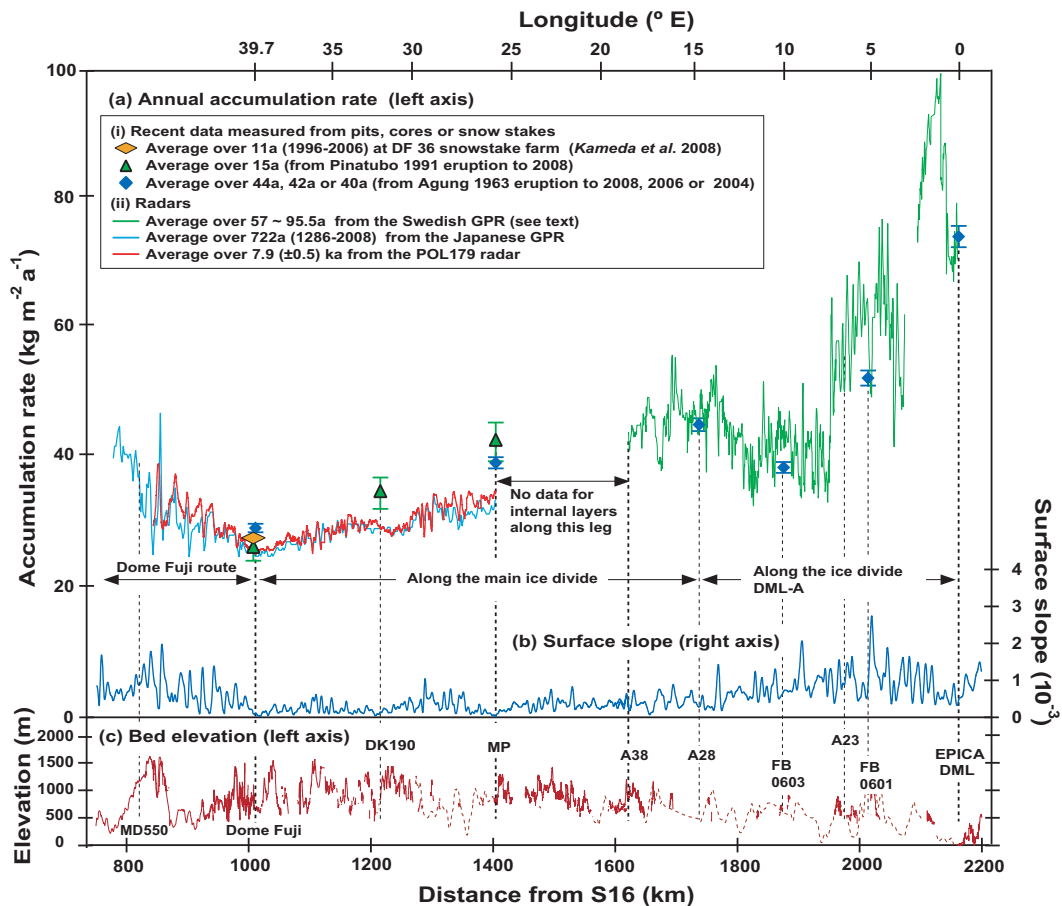
Fig. 3. Annual accumulation rates over various time scales are shown with indicators of the depositional environment along the main route of the traverse. The abscissa represents distance from S16 along the traverse route. Details are as follows. **(a)** Annual accumulation rate averaged over various time scales. Pit studies and firn core studies provided accumulation rates averaged over 44 yr and/or 15 yr (see text). Also shown is the annual accumulation rate averaged over 11 yr from 1996 to 2006 (Kameda et al., 2008) from a stake farm with 36 stakes at Dome Fuji. Subsurface radars provide annual accumulation rates averaged over 57–96 yr, ∼722 yr and 7.9 k yr. Details are given in the text. **(b)** Surface slope at each point along the route was calculated using the digital elevation model of Bamber et al. (2006). **(c)** Bed elevation derived from radar sounding.

surface slope and bed elevation (Fig. 9b, c and d, respectively). The accumulation rate data were again derived from the Japanese GPR and the POL179 radar data that give a 722 a average and a 7.9 ka average, respectively. The gradients across the ice divide are steep, -0.30 $(\mathrm{kg\,m^{-2}\,a^{-1})\,km^{-1}}$ (decreasing toward the inland part of the ice sheet) for the 722 a average and -0.18 $(\mathrm{kg\,m^{-2}\,a^{-1})\,km^{-1}}$ for the 7.9 ka average. To further clarify these results, a contour map was made using data for the annual accumulation rate averaged over 722 a for an area between Dome Fuji and MP, including the cross-ice divide survey at MP, and this is shown in Fig. 10. Because our purpose was to visualize large-scale trends in the gradient, for most of the traverse routes the original data was smoothed over a 40-km distance to reduce fluctuations. For the 40-km-long cross-ice divide traverse at MP, a regression line was used. It can be seen that the gradient in

the vicinity of MP is much steeper than that in the vicinity of Dome Fuji. The reason for this will be discussed in the next section.

4.1.2 Large-scale trend inferred from passive microwave data

To further clarify the large-scale trend in the accumulation rate, data from the passive microwave measurements are useful. The data features itemized in Sect. 3.3 will now be addressed individually.

i. In general, the NE region exhibits higher PR6.9 values than the SW region.

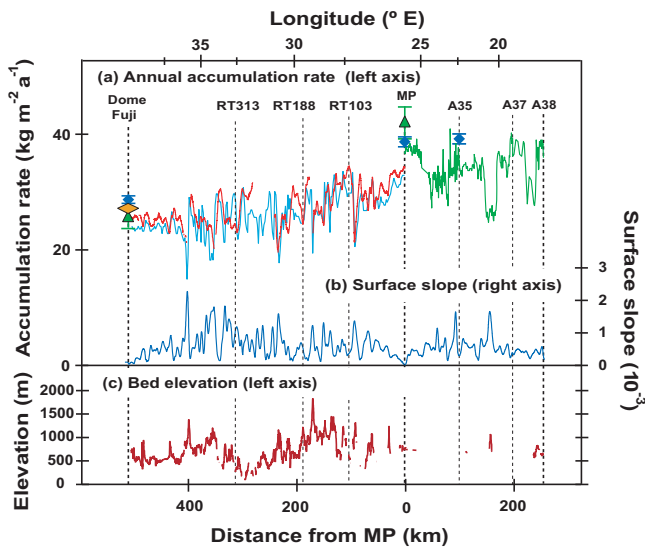ii. In the area between Dome Fuji and MP, a PR6.9 gradient occurs across the ice divide. In fact, the PR6.9

Fig. 4. Annual accumulation rate over various time scales are shown with indicators of the depositional environment along the south route. Again, surface slopes and bed elevation are shown as in Fig. 3. The abscissa indicates distance from MP along the traverse route. All other items and symbols are the same as in Fig. 3. Fluctuations of the accumulation rate and surface slope are much larger than those along the route in the main ice divide.

distribution agrees well with the distribution of the accumulation rate shown in Fig. 10, suggesting that PR6.9 is well correlated with the accumulation rate in this region, at least qualitatively. At MP, the steep PR6.9 gradient across the ice divide agrees well with that of the accumulation rate, as seen in Figs. 9 and 10. These facts suggest that the main ice divide in DML is a location where a rapid change in the SMB occurs.

iii. The leg between A28 and EPICA DML is within the high PR6.9 zone, which is possibly linked to a lower accumulation rate. However, Fig. 3 shows that the accumulation rate in this area is higher than that along the main ice divide. Since the PR at frequencies below 10 GHz has been found to be a good indicator of the number of strata in the snow cover (Surdyk and Fily, 1993, 1995), this implies that there must be some other factors causing the large number of strata in this area. A plausible explanation is the frequent occurrence of dune formation events. Birnbaum et al. (2010) investigated dune layers from past formation events in nine 5-m-long firn cores adjacent to EPICA DML. They identified 6–12 buried snow-dune layers per core, suggesting an unexpectedly large stratification. Indeed, snow stratification is more disturbed by wind in this area than it is in the main ice divide. As can be seen in Fig. 5, multiple orientations of snow surface reliefs are present. In addition, the accumulation rate is highly variable (Figs. 3a

and 8a). Moreover, we found that the received radar signals from within the shallow (∼200 m) part of the ice sheet were weaker by 5–10 dB than those along the main ice divide (data not shown). These data imply that the effect of wind on the surface snow strata causes a reduction in TB_h. This hypothesis also explains why PR6.9 is very high in the SE of EPICA DML where the downslope katabatic wind is expected to be stronger. To further examine this possibility, we need to compare the number of buried strata in different regions.

iv. The eastern and north-eastern sides of the ice divide branches (from DML-A to DML-E) tend to have higher accumulation rates, whereas the opposite sides tend to have lower accumulation rates.

v. The route of the Norwegian-USA traverse is almost entirely on the side with relatively high PR6.9 values. This means that the data from this traverse reflect a depositional environment characterized by relatively high PR6.9 values and hence relatively low accumulation rates.

In summary, the PR6.9 map provides insights into the distribution of snow strata in this area and its association with the accumulation rate and presumably dune formation. Qualitatively, the PR6.9 distribution agrees well with the accumulation rate data in the vicinity of the main ice divide. In the vicinity of EPICA DML, PR6.9 is likely to be affected by an increased roughness and/or increased number of strata due to the higher frequency of dunes per unit thickness of firn. Further work should include an analysis of local variability, quantitative analysis, and the development of theoretical models and algorithms to derive the accumulation rate from the PR data.

4.1.3 Local-scale variability

We next examine local variability of the annual accumulation rate. In addition to the large-scale trend discussed above, local topography has a strong influence on local variability. On this scale, we find that there is an anticorrelation between the accumulation rate and the surface slope along the JASE traverse (Figs. 3, 4, 8 and 9). This suggests that snow is more easily deposited on a relatively flat surface, particularly if it is somewhat concave (see locations at −12 km and +10 km in Fig. 9a, b for example). We suggest that one of the major controlling factors of local variability is the surface slope, as pointed out in earlier studies. In addition, surface slope is highly correlated to bedrock topography, as can be seen from Figs. 3, 4 and 9. Thus, local variations in the accumulation rate are naturally preserved over time. That is, locally high or low accumulation sites tend to remain so over long time scales. In this study, we observed that the spatial variabilities of the 722 a and 7.9 ka average accumulation rates are very similar, both along the main ice divide (Fig. 3a) and along the
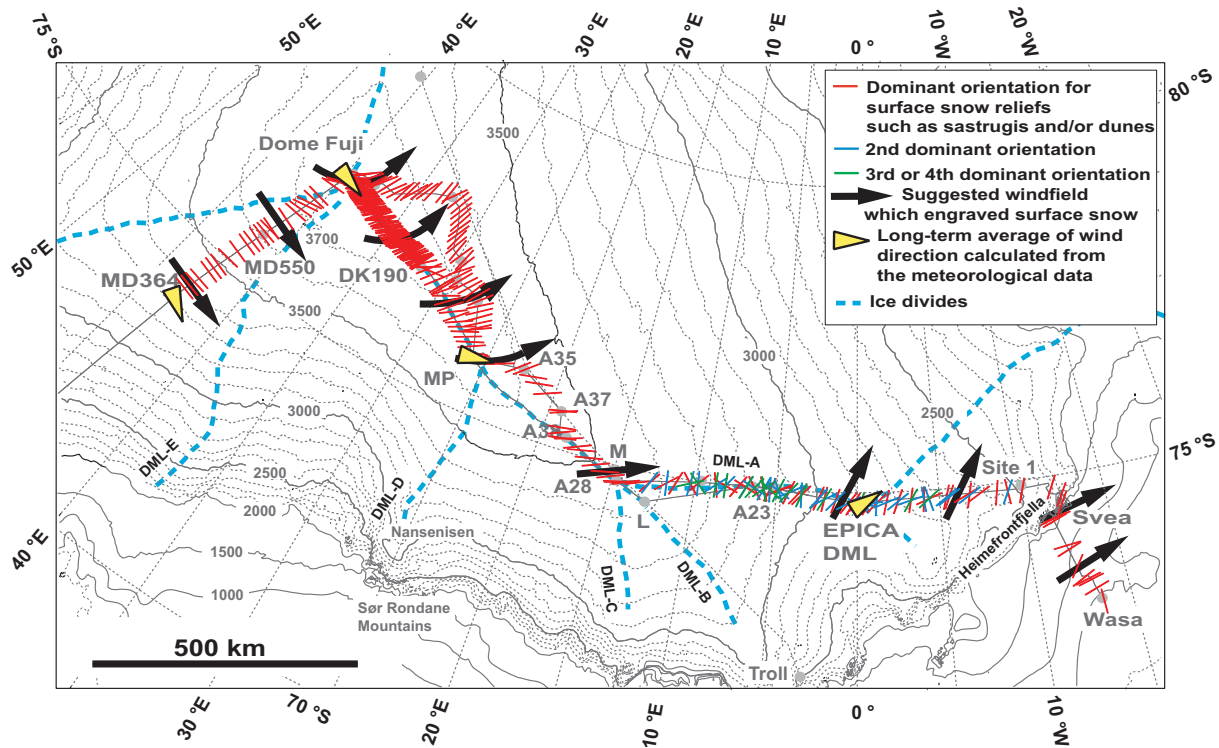
Fig. 5. Dominant orientation of surface snow reliefs such as sastrugis and dunes observed along the traverse routes between MD364 and Wasa. Orientations are plotted as thin lines on the map. At some sites, two or more orientations were observed, in particular at sites between A28 and A23. The dominant orientation is shown as red symbol markers. The second and lesser orientations are shown as green and blue markers, respectively. Thick black arrows are the suggested directions of the strong winds ($>\sim 10\,\mathrm{m\,s^{-1}}$) that caused the surface snow reliefs. Yellow arrows represent the orientation of the average wind field at MD364, DF, MP and EPICA DML, calculated from the meteorological data. For MD364, DF and MP, the yellow arrows show the directions of the average wind vectors. Details are given in Table 4. At EPICA DML, the yellow arrow represents the long-term average wind direction (Birnbaum et al., 2010; Reijmer and Van den Broeke, 2003). Bold blue dashed curves indicate ice divides.

south route (Fig. 4a). This is basically due to preservation of the accumulation pattern over these time scales. To determine the depositional history in more detail would require a knowledge of the ice-flow trajectory in these regions.

4.2 Influence of strong-wind events on spatial distribution of SMB

4.2.1 Reasons to expect a link between SMB and strong-wind events

We next discuss the relation between strong-wind events observed in the data (both AWS and snow surface reliefs) and snow accumulation. Earlier papers by Schlosser et al. (2008, 2010) provided useful summaries of the current understanding of the relation between precipitation and SMB in DML. Table 5 gives a summary of the SMB components in Antarctica, based on the results of earlier studies (e.g., Bromwich, 1988; Bromwich et al., 2004; Schlosser et al., 2008, 2010). Generally, on the Antarctic ice sheet, the SMB is the differ-

ence between the amount of surface accumulation and ablation. Accumulation mechanisms include precipitation, hoarfrost deposition, and deposition of snow due to snowdrift, whereas ablation mechanisms include sublimation and wind erosion due to snowdrift. Sublimation can occur both during and after snowfall and snowdrift. Among the many factors influencing the SMB of the Antarctic ice sheet, precipitation is recognised as the most important component.

As summarized above and in the introduction, the SMB is not simple to determine because the roles of its components can vary both spatially and temporally. Nevertheless, it should be emphasized that episodic precipitation events are in many cases associated with increased wind speed and temperature (e.g., Birnbaum et al., 2010; Fujita and Abe, 2006; Schlosser et al., 2008, 2010; Hirasawa, 2010), implying synoptic-scale advection of air masses from lower latitudes. Fujita and Abe (2006) presented time-series data for precipitation events at Dome Fuji for 2003. We compared their data with meteorological data (Japan Meteorological Agency, 2005) obtained at Dome Fuji during the
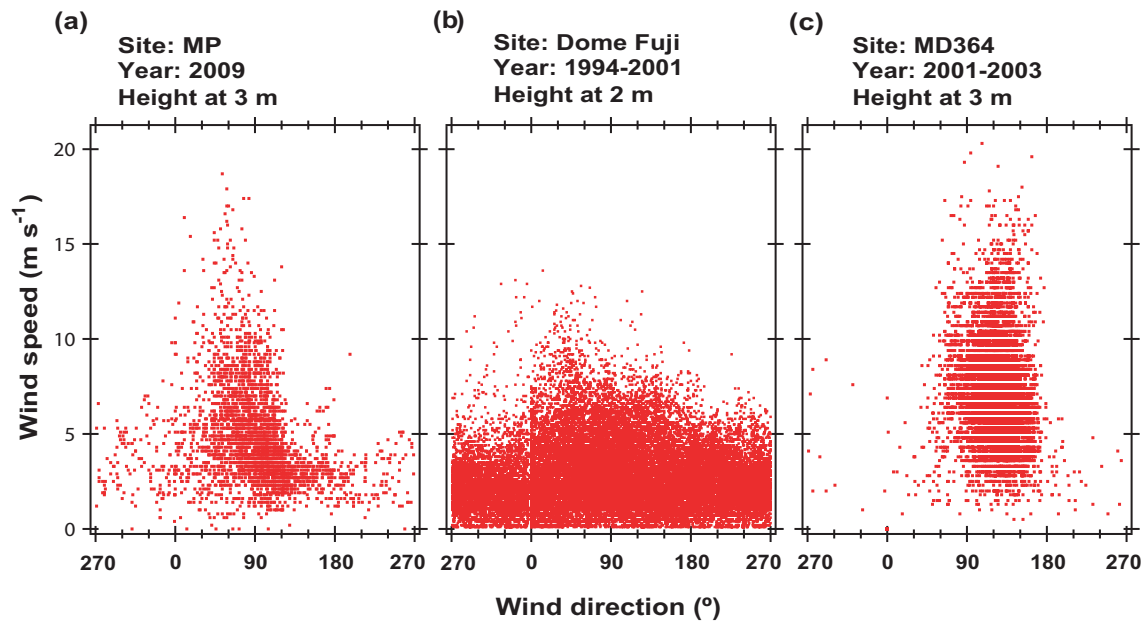
Fig. 6. Relationship between wind speed and direction at the three AWS sites along the JASE traverse. **(a)** Data at MP during the year 2009. The observational data is from the AWS JASE2007. Data selected at three hourly intervals were used. Of the measured events, 6 % have wind speeds of more than 10 m s^{-1}, with an average wind direction of 70° (±24°, standard deviation). **(b)** Data at Dome Fuji during the years from 1994 to 2001 (Takahashi et al., 2004). Data at hourly intervals were used. Of the measured events, 1 % has wind speeds of more than 8 m s^{-1}, with an average wind direction of 53° (±48°). **(c)** Data at MD364 during the years from 2001 to 2003 (Keller et al., 2010). Data at three hourly intervals were used. Of the measured events, 14 % have wind speeds of more than 10 m s^{-1}, with an average wind direction of 120° (±22°).

same time period and the results are shown in Fig. 11. Daily (more accurately, 24 h) precipitation (Fujita and Abe, 2006) is plotted versus wind speed (Fig. 11a) and direction (Fig. 11b). Figure 11a shows that high-precipitation events are associated with strong-wind events in most cases. Most high-precipitation events occurred with a limited range of near-surface wind direction centered on 55° (±25°). This direction is the same as that of the strongest winds observed in meteorological data over a much longer time span from 1994 to 2001 (see Fig. 6b and Table 4). This implies that in many cases strong winds directly distribute the precipitation during high-precipitation events. In addition, high-precipitation/strong-wind events are characterized by advection of maritime air masses from relatively lower latitudes (e.g., Birnbaum et al., 2010; Schlosser et al., 2010; Hirasawa et al., 2000). Thus, these events are keys for understanding the distribution of maritime moisture onto the ice sheet surface. Although in some cases, strong-wind events are not directly accompanied by snow precipitation, strong winds can redistribute snow soon after it is deposited. Therefore, we consider strong-wind events to have an important influence on the SMB distribution. In lower-elevation regions further from the ice divides, katabatic winds become progressively stronger and thus have a larger influence on the depositional environment, particularly in terms of the redistribution of

drifted snow. These effects have been discussed in detail in earlier papers (e.g., Frezzotti et al., 2005, 2007; Urbini et al., 2008).

4.2.2 Interpretation of surface snow reliefs

We now examine the relationship between the wind field associated with strong-wind events and the spatial distribution of the SMB. A question arises as to how the dominant orientations of the surface snow reliefs reflect the wind field. Although the orientation of surface relief may not necessarily represent the persistent prevailing wind direction, we contend that it is not simply associated with the most recent storm. This is supported by the fact that the azimuthal dependence of AMSR-E microwave emissivity exhibits little seasonality (S. Surdyk, unpublished work). However, since the observational data used in the present study were obtained within a limited time period during an inland traverse, a more comprehensive analysis of satellite remote sensing data is required to address this question. In this regard, useful information can be found in the AWS data shown in Fig. 6. There is a sharp peak in the wind speed - direction plot, suggesting that the relief orientations are persistent. The wind direction during stronger wind events should have a larger effect. Less strong winds with directions deviating from those of
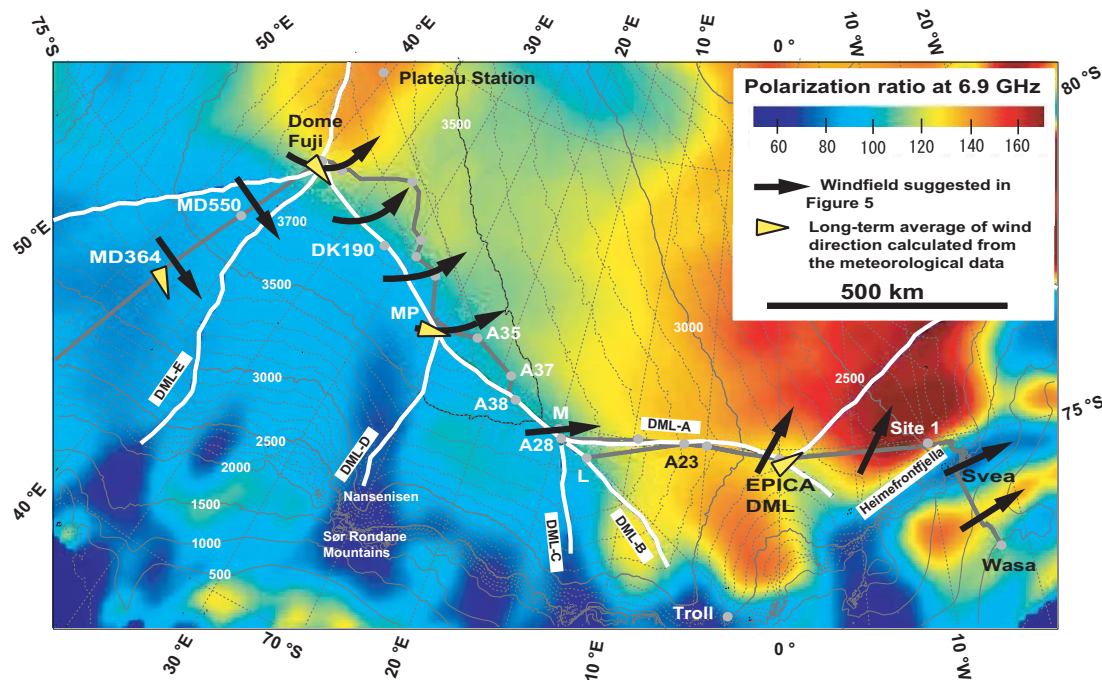
Fig. 7. Distribution of the polarization ratio of passive microwave data at 6.9 GHz. Data were obtained from the Advanced Microwave Scanning Radiometer for EOS (AMSR-E), which was developed by JAXA for use on board the EOS satellite that has been operating since 2002. Previous studies (Surdyk and Fily, 1993, 1995) suggested that the polarization ratio at frequencies lower than 10 GHz is an indicator of the number of layers per unit depth of strata to a depth of ~2 m. Lower/higher values mean fewer/more layers in the strata, which would qualitatively suggest that the accumulation rate is higher/lower. In the area between Dome Fuji and MP, the distribution of the polarization ratio closely resembles that of the accumulation rate shown in Fig. 10. The ice divide branch DML-A between site A28 and EPICA DML is within an area of higher polarization ratio. In addition, the legs of the Norwegian-USA traverse from Troll Station to Plateau Station is also within an area of higher polarization ratio.

the strongest winds can still redistribute snow but have less ability to engrave the snow surface. Therefore, we assume that the dominant orientations of the surface snow reliefs "most probably" represent the wind field associated with the strongest winds, as seen in Fig. 6.

4.2.3 Direction of the wind field that engraved the snow surface

Based on the surface snow reliefs, we deduced the directions of the wind fields that engraved the snow surface, and these are shown as thick black arrows in Fig. 5. Near ice divides, the directions are around ENE, so that the wind clearly crosses the ice divides. Along the route between A28 and A23, snow reliefs with multiple different orientations were observed. This suggests that the wind in this area was variable, at least for some period before the observations were carried out. Since all of the observations in this area were performed by the same individual, fluctuations in the data quality are unlikely to be a factor here. As was pointed out in Sect 4.1.2(iii), the strata in this area exhibited different characteristics to those along the main ice divide. Thus, we hy-

pothesize that the multiple orientations of the surface reliefs are typical features of the snow surface in this area.

At MP, Dome Fuji and EPICA DML, the directions of the strongest near-surface winds agree well with the dominant orientations of the surface snow reliefs. They deviate from the average wind vectors indicated by yellow arrows in Fig. 5 toward the northeast or even further northwards. At MD364, the observed orientation of surface snow features is ~102° which is within the range of variation of the wind direction for strong-wind events, 120° ± 22° (see Table 4). We note that this site is strongly influenced by katabatic winds.

Finally, the thick black arrows in Fig. 5 represent the most probable directions of the strongest wind at each site, are also consistent with the AWS data. Most high-precipitation events occur when the wind has these directions, at least at Dome Fuji and presumably at other sites. The SMB in DML is highly influenced by these near-surface wind directions, as will be further discussed below.
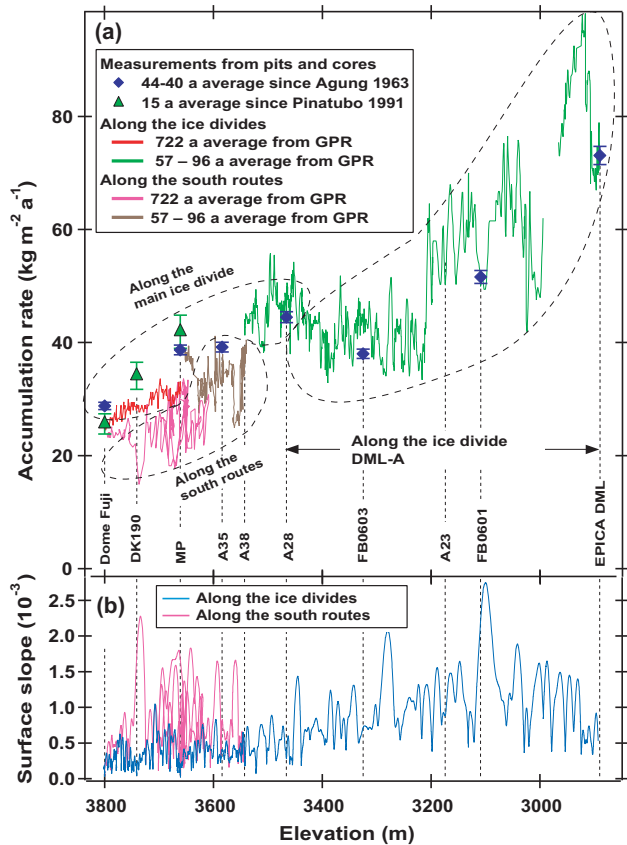
Fig. 8. Values of accumulation rate are shown versus site elevation. Panel **(a)** shows data selected from Figs. 3a and 4a. The group in the upper left is data from sites along the main ice divide between Dome Fuji and A28. The group at the lower left side is data from sites along the south route between Dome Fuji and A38. The group on the right side is data from sites along the ice divide branch DML-A between A28 and EPICA DML. Panel **(b)** shows surface slope.

Fig. 9. Annual accumulation rate for the 40-km-long cross-ice divide survey at MP. **(a)** Annual accumulation rates averaged over 7.9 ka (red trace) and 722 a (blue trace) are determined from subsurface radar data. They are compared with the average over 44 a at MP. Also shown are **(b)** surface elevation, **(c)** surface slope, and **(d)** bed elevation. Decrease in accumulation rate from the northern coastal side of the ice divide toward the southern interior side. The annual accumulation rate is locally higher at locations with flat or concave surface topography, as indicated by thin vertical dashed lines. Similarly, the annual accumulation rate is locally lower at locations with steep surfaces or a convex surface topography.

4.2.4 Widespread strong upslope winds in DML during strong-wind events

Earlier studies have also shown that strong-wind events are often associated with wind directions between north and east. Watanabe (1978) identified two different wind systems using data for 1977 at Mizuho Plateau in DML: one is almost always directed approximately 60-90° counterclockwise from the downslope direction, while the other has a larger counterclockwise tilt, even pointing upslope in the dome area at high latitudes. Watanabe (1978) suggested that the former represents the katabatic wind which prevails over the gently sloping ($2 \sim 3 \times 10^{-3}$) plateau area, while the other is caused by severe snowstorms characterized by strong winds. In addition, Kikuchi (1997) found that the wind fields during blizzards had upslope components and were widely observed in an area between 30° E and 50° E in DML. Birnbaum et al. (2010) suggested that all strong-wind and, hence,

all barchan-type dune formation events at EPICA DML identified in a 7 yr period were caused by the influence of a low-pressure system. They also found that in the majority of strong-wind and dune formation events, the near-surface wind turned counterclockwise. Birnbaum et al. (2010) further suggested that enhanced katabatic flow is not the reason for the unusually high near-surface wind speeds at EPICA DML, which is in accordance with the findings by Van As et al. (2007) that the largest near-surface wind speeds at EPICA DML are caused by strong large-scale forcing. These earlier studies and the thick black arrows in Fig. 5 suggest that the northeastern sides of the ice divides are the windward sides during strong-wind events, where upslope wind often occurs. The strong winds cross the ice divides and blow down their southern and southwestern slopes.
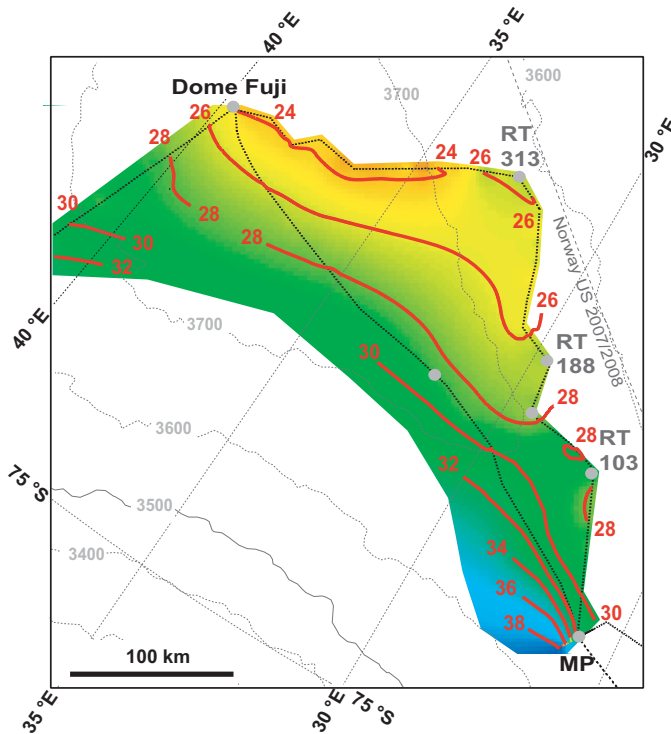
Fig. 10. Map of annual accumulation rate averaged over 722 a, derived from the GPR data. Colour scale image with bold red contours and red letters shows the distribution of the accumulation rate in $kg\,m^{-2}\,a^{-1}$. Surface elevation of the ice sheet is also shown by thin gray contour lines. The purpose of this map is to visualize the large-scale spatial distribution of the accumulation rate in this area. For this purpose, the original data was smoothed over a distance of 40 km to reduce fluctuations. Annual accumulation rates averaged over 749 a at the NUS07-2 and NUS07-5 sites are listed in Table 3c for comparison.

4.2.5 Large-scale distribution of SMB at and around ice divides

We hypothesize that many of the features of the SMB and PR6.9 distributions are explainable primarily by strong-wind and high-precipitation events. These events are often associated with advection of air masses from relatively low latitudes inland across the ice divides. Because of the upslope direction of the near-surface winds, such air masses release most of their moisture due to orographic lift on the windward sides of the ice divides. After the winds cross the ice divides, the leeward side basically corresponds to the rain shadow; subsequent adiabatic warming of dry air can occur for downslope winds in the leeward area. Multiple ice divides along paths of strong winds can make the air mass progressively drier. The relatively low accumulation rate in the leg between A28 and A23 (Figs. 3a and 8a) can be understood in terms of the geographical location of the sites in DML. The ice divide branch DML-A is located on the lee-

ward side of the two ice divides DML-C and DML-B, and is thus in their rain shadow. It seems likely that the snow reliefs with multiple orientations along this leg are caused by the complex wind field on the lee of these multiple ice divides. The escarpment between the low-altitude coastal areas and the interior plateau causes local minima and maxima in precipitation, which correspond to the leeward and windward sides of topographical ridges. This situation was also studied by Schlosser et al. (2008) based on Antarctic Mesoscale Prediction System (AMPS) archive data. An interesting feature is the strong PR6.9 contrast along the Heimefrontfjella (Fig. 7). It implies that there is a high-accumulation-rate corridor at the foot of the Heimefrontfjella, with the interior of the plateau having a lower accumulation rate. Indeed, the Heimefrontfjella follows the strong wind direction. The SMB at the foot of the polar plateau is high ($\sim$200 $\pm$60 $kg\,m^{-2}\,a^{-1}$) whereas that on the polar plateau is low ($\sim$60 $\pm$20 $kg\,m^{-2}\,a^{-1}$) near Site 1, (Richardson et al., 1997).

Apart from precipitation due to high-precipitation events, several other components in Table 5 contribute to the SMB. Some of these have a larger effect further from the ice divides at lower elevations on the polar plateau. For example, several papers have pointed out that wind-driven ablation is determined by the surface slope along the wind direction (e.g., Frezzotti et al., 2004). Frezzotti et al. (2004) investigated the SMB along a transect from Terra Nova Bay to Dome C in East Antarctica. They found that the measured maximum snow accumulation rate is well correlated to firn temperature. They suggested that wind-driven sublimation processes, controlled by the surface slope in the wind direction, have a huge impact (up to 85 % of snow precipitation) on the SMB. They further suggested that the snow redistribution process is local and has a strong impact on the annual variability of accumulation rate. Analogous phenomena would be expected to occur in DML. Determining the role of wind-driven sublimation processes in DML requires an analysis of the wind system (e.g., Van den Broeke and Van Lipzig, 2003), including both strong-wind events and katabatic winds, the local topography of the ice sheet surface and the orientation of snow surface reliefs.

4.3 Increase in accumulation rate during the 20th century

Figures 3a, 4a and 9a show a comparison of the annual accumulation rate over different periods of time within the late Holocene. We find that in the $\sim$500-km-long leg between Dome Fuji and A35, the average accumulation rates after 1964 AD (the Agung 1963 eruption) and/or after 1993 (the Pinatubo 1991 eruption) are significantly higher than accumulation rates averaged over longer periods (722 a and 7.9 ka). These data suggest an increase in the accumulation rate, at least during the second half of the 20th century, in the sector between 40° E and 22.5° E.
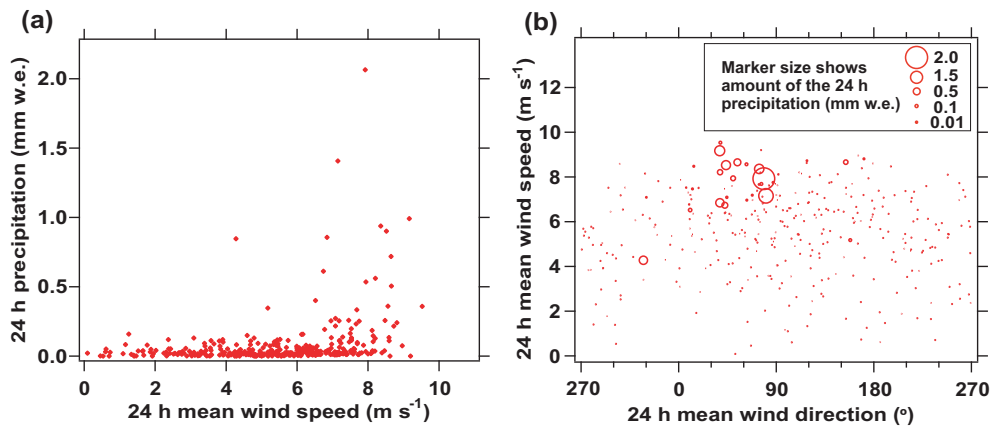
Fig. 11. Relation between high-precipitation events and strong-wind events at Dome Fuji Station in a period from February 2003 to January 2004. The amount of precipitation each 24 hours was measured (Fujita and Abe, 2006). Wind speed and direction was measured at a height of 10 m above the ground (Japan Meteorological Agency, 2005). Each data point represents an average over 24 h. Correlations were then investigated. **(a)** Relation between 24-h precipitation (in mm, water equivalent) and 24-h-mean wind speed. High-precipitation events are associated with strong-wind events in most cases. **(b)** Relation between 24-h-mean wind speed (same as in (a)) and 24-h-mean wind direction. Size of the marker represents the amount of precipitation. Most high-precipitation events occured with a limited range of wind direction centered at 55° (±25°). This direction agrees well with the direction of the strongest winds (see Fig. 6b and Table 4).

Contrasting results have been reported for the legs of the Norwegian-USA scientific traverse in the vicinity of the JASE traverse routes. Anschütz et al. (2011) investigated the spatio-temporal accumulation pattern based on volcanic signatures in ice-core records. They investigated 13 firn cores from the Norwegian-USA traverse including five sites (NUS07-1 to 07-5) in Fig. 1. Major volcanic eruptions were identified and used to assess century-scale accumulation rate changes. They reported that the largest changes seemed to occur in the most recent decades with the accumulation rate in the period 1963–2007/08 being up to 25 % different from the long-term record. They also reported that there was no clear overall trend; some sites showed an increase in accumulation rate over the period 1963 to present while others showed a decrease. The data from almost all sites that are 3200 m or more above sea level suggested a decrease in accumulation rate, including sites NUS07-1 to 07-5. Some of their data are given in Table 3c for comparison to the data of the JASE traverse . From the viewpoint of the influence of strong-wind events on the spatial distribution of the SMB, we note that all of the sites on the Norwegian-USA traverse are located on the leeward side of the ice divides.

As described in Sect. 1.2, there have been many regional studies in Antarctica that reported an increase in the SMB during the 20th century. In the majority of earlier reports and also in the present study, a trend towards increasing accumulation rates during the 20th century is commonly found for the polar plateau, near Dome Fuji, EPICA DML, sites along the ice divide between them, the South Pole, Dome C and Talos Dome. However, no significant change was reported for other sites, mostly along the legs of the Norwegian-USA

travese connecting Troll Station, A28, Plateau Station and further inland. Because these sites are all located on the leeward sides of ice divides, we hypothesize that the locations of these sites possibly mask any increase in accumulation rate. Even if moisture transport toward the interior increases, it is plausible that the majority of the moisture is released due to the windward effect. To further investigate spatially inhomogeneous changes in the SMB, we suggest that cross-ice divide surveys connecting the windward and leeward sides would be effective.

5 Concluding remarks

In the JASE traverse, we investigated spatial and temporal variability of the ice sheet environment in the sparsely explored inland plateau area of East Antarctica. The major findings of the present study are summarized as follows.

1. On the inland plateau of DML, the prevailing wind direction associated with strong-wind events agreed well with the orientation of surface snow reliefs. We suggest that high-precipitation events associated with strong-wind events have a major influence on the spatial distribution of the SMB. Strong winds often have upslope components in DML causing advection of air masses from relatively low latitudes over DML. It is suggested that strong winds with upslope components release their moisture on the windward side of the ice divide and the leeward side is then exposed to drier air. As a result, a different SMB is found on the windward and leeward sides of the ice divides. Although there are several other

components comprising the SMB (see Table 5), high-precipitation events with strong winds seem to be the most influential. The effect of wind-driven ablation is something that needs to be assessed in the future.

2. In the scenario described above, large-scale variations in the SMB depend on surface elevation, continentality and location of sites with respect to the ice divides in DML.

3. Local variations in the SMB are essentially governed by the local surface topography, which in turn is influenced by the bedrock topography. Thus, the spatial pattern of the accumulation rate was unchanged over the investigated periods along the main ice divide route and the south route. Spatial variability of the accumulation rate is smaller along the ice divide than in regions away from the ice divide, suggesting an advantage of using ice divide areas for studying temporal variations in the paleoclimatic signals from ice cores.

4. In the eastern part of DML at longitudes from ∼15° E to ∼40° E, the accumulation rate in the second half of the 20th century is found to be higher by ∼15 % compared to averages over longer periods of 722 a and 7.9 ka. This recent increase in accumulation rate is consistent with reports of studies on many sites in the inland plateau of East Antarctica. However, some studies have indicated insignificant increases at sites commonly in the lee of ice divides. We suggest that the geographical location of these sites on the leeward side of the ice divide may lead to any increase in the accumulation rate being masked. The increase in the accumulation rate in the second half of the 20th century is a topic that should be examined by climatologists in the context of climate change and global warming.

5. In addition to the new SMB data, a new data set for ice sheet thickness was produced as shown in the figures. This will be used for a future international compilation of an ice sheet topography map. Moreover, a new data set was produced for snow surface reliefs, and meteorological data is available from the JASE2007 AWS at MP.

6. The polarization ratio at 6.9 GHz derived from the passive microwave data is found to be well correlated with the accumulation rate data in the vicinity of the main ice divide, at least from a qualitative point of view. This provides insights into the large-scale trend of the accumulation rate. However, near EPICA DML, PR6.9 is likely to be affected by increased roughness and/or increased number of strata due to the higher frequency of dunes per unit thickness within the firn. Based on the results of previous studies on the polarization ratio (Surdyk and Fily, 1993, 1995), PR6.9 is thought to be a good indicator of stratification in the snow cover.

References

Alley, R., Clark, P., Huybrechts, P., and Joughin, I.: Ice-sheet and sea level changes, Science, 310, 456–460, doi:10.1126/science.1114613, 2005.

Anschütz, H., Müller, K., Isaksson, E., McConnell, J. R., Fischer, H., Miller, H., Albert, M., and Winther, J.-G.: Revisiting sites of the South Pole Queen Maud Land Traverses in East Antarctica: Accumulation data from shallow firn cores, J. Geophys. Res., 114, D24106, doi:10.1029/2009JD012204, 2009.

Anschütz, H., Sinisalo, A., Isaksson, E., McConnell, J. R., Hamran, S.-E., Bisiaux, M. M., Pasteris, D., Neumann, T. A. and Winther, J.-G.: Variation of accumulation rates over the last eight centuries on the East Antarctic Plateau derived from volcanic signals in ice cores, J. Geophys. Res., 116, D20103, doi:10.1029/2011JD015753, 2011

Arthern, R. J., Winebrenner, D. P., and Vaughan, D.G.: Antarctic snow accumulation mapped using polarization of 4.3-cm wavelength microwave emission, J. Geophys. Res, 111, D06107, doi:10.1029/2004JD005667, 2006.

Bamber, J. L., Gomez-Dans, J. L., and Griggs, J. A.: Antarctic 1 km Digital Elevation Model (DEM) from Combined ERS-1 Radar and ICESat Laser Satellite Altimetry, in: National Snow and Ice Data Center. Digital media, Boulder, Colorado USA, 2009.

Birnbaum, G., Freitag, J., Brauner, R., König-Langlo, Schulz, G. E., Schulz, E., Kipfstuhl, S., Oerter, H., Reijmer, C. H., Schlosser, E., Faria, S. H., Ries, H., Loose, B., Herber, A.,

Duda, M. G., Powers, J. G., Manning, K. W., and Van den Broeke, M. R.: Strong-wind events and their influence on the formation of snow dunes: Observations from Kohnen Station, Dronning Maud Land, Antarctica, J. Glaciol., 56, 891–902, doi:10.3189/002214310794457272, 2010.

Braaten, D. A.: Direct measurements of episodic snow accumulation on the Antarctic polar plateau, J. Geophys. Res., 105, 10,119–10,128, doi:10.1029/2000JD900099, 2000.

Bromwich, D. H., Snowfall in high southern latitudes, Rev. Geophys., 26, 149–168, doi:10.1029/RG026i001p00149, 1988.

Bromwich, D. H., Guo, Z., Bai, L., and Chen, Q.-S.: Modeled Antarctic precipitation. Part I: Spatial and temporal variability, J. Climate, 17, 427–447, doi:10.1175/1520-0442(2004)017<0427:MAPPIS>2.0.CO;2,2004.

Chen, J., Wilson, C., Blankenship, D., and Tapley, B.: Antarctic mass rates from GRACE, Geophys. Res. Lett., 33, L11502, doi:10.1029/2006GL026369, 2006.

Cole-Dai, J., Mosley-Thompson, E., and Thompson, L. G.: Quantifying the Pinatubo volcanic signal in south polar snow, Geophys. Res. Lett., 24 (21), 2679–2682, doi:10.1029/97GL02734, 1997.

Cullather, R. I., Bromwich, D. H., and Van Woert M. L.: Spatial and temporal variability of Antarctic Precipitation from atmospheric methods, J. Climate, 11, 334–367, 1998.

Davis, C., Li, Y., McConnell, J., Frey, M., and Hanna, E.: Snowfall-driven growth in East Antarctic ice sheet mitigates recent sea-level rise, Science, 308, 5730, 1898–1901, doi:10.1126/science.1110662, 2005.

Eisen, O., Frezzotti, M., Genthon, C., Isaksson, E., Magand, O., Van den Broeke, M. R., Dixon, D.A., Ekaykin, A., Holmlund, P., Kameda, T., Karlöf, L., Kaspari, S., Lipenkov, V., Oerter, H., Takahashi, S., and Vaughan, D. G.: Ground-based measurements of spatial and temporal variability of snow accumulation in East Antarctica, Rev. Geophys., 46, RG2001, doi:10.1029/2006RG000218, 2008.

Endo, Y. and Fujiwara, K.: Characteristics of the snow cover in East Antarctica along the route of the JARE South Pole traverse and factors controlling such characteristics, Polar Res. Cent., Natl. Sci. Mus., Tokyo, 38 pp., 1973.

EPICA Community Members: One-to-one coupling of glacial climate variability in Greenland and Antarctica, Nature, 444, 195–198, doi:10.1038/nature05301, 2006.

Frezzotti, M., Pourchet, M., Flora, O., Gandolfi, S., Gay, M., Urbini, S., Vincent, C., Becagli, S., Gragnani, R., Proposito, M., Severi, M., Traversi, R., Udisti, R., and Fily, M.: New estimations of precipitation and surface sublimation in East Antarctica from snow accumulation measurements, Climate Dynamics, 23, 803–813, doi:10.1007/s00382-004-0462-5, 2004.

Frezzotti, M., Pourchet, M., Flora, O., Gandolfi, S., Gay, M., Urbini, S., Vincent, C., Becagli, S., Gragnani, R., Proposito, M., Severi, M., Traversi, R., Udisti, R., and Fily, M.: Spatial and temporal variability of snow accumulation in East Antarctica from traverse data, J. Glaciol., 51, 113–124, doi:10.3189/172756505781829502, 2005.

Frezzotti, M., Urbini, S., Proposito, M., Scarchilli, C., and Gandolfi, S.: Spatial and temporal variability of surface mass balance near Talos Dome, East Antarctica, J. Geophys. Res., 112, F02032, doi:10.1029/2006JF000638, 2007.

Fujita, K., and Abe, O.: Stable isotopes in daily precipitation at Dome Fuji, East Antarctica, Geophys. Res. Lett., 33, L18503,

doi:10.1029/2006GL026936, 2006.

Fujita, S., Maeno, H., Uratsuka, S., Furukawa, T., Mae, S., Fujii, Y., and Watanabe, O.: Nature of radio-echo layering in the Antarctic ice sheet detected by a two-frequency experiment, J. Geophys. Res., 104(B6), 13013–13024, doi:10.1029/1999JB900034, 1999.

Fujita, S., Matsuoka, T., Ishida, T., Matsuoka, K., and Mae, S.: A summary of the complex dielectric permittivity of ice in the megahertz range and its applications for radar sounding, in: Physics of Ice Core Records, edited by: Hondoh, T., Hokkaido University Press, Sapporo, 185–212, 2000.

Fujita, S., Azuma, N., Motoyama, H., Kameda, T., Narita, H., Fujii, Y., Watanabe, O.: Electrical measurements from the 2503-m Dome F Antarctic ice core, Ann. Glaciol., 35, 313–320, doi:10.3189/172756402781816951, 2002a.

Fujita, S., Maeno, H., Furukawa, T., and Matsuoka, K.: Scattering of VHF radio waves from within the top 700 m of the Antarctic ice sheet and its relation to the depositional environment: a case study along the Syowa-Mizuho-Dome F traverse, Ann. Glaciol., 34, 157–164, doi:10.3189/172756402781817888, 2002b.

Fujita, S., Enomoto, H., Kameda, T., Motoyama, H., and Sugiyama, S.: Changes of surface snow density in a summer in the Antarctic Dome Fuji region, paper presented at SCAR/IASC IPY Open Science Conference, Assoc. of Polar Early Career Sci., St. Petersburg, Russia, 8–11 July 2008.

Furukawa, T., Kamiyama, K., and Maeno, H.: Snow surface features along the traverse route from the coast to Dome Fuji Station, Queen Maud Land, Antarctica, Proc. NIPR Symp. Polar Meteorol. Glaciol., 10, 13–24, 1996.

Giovinetto, M. and Zwally, H.: Spatial distribution of net surface accumulation on the Antarctic ice sheet, Ann. Glaciol., 31, 171–178, doi:10.3189/172756400781820200, 2000.

Göktas, F., Fischer, H., Oerter, H., Weller, R., Sommer, S., and Miller, H.: A glacio-chemical characterisation of the new EPICA deep-drilling site on Amundsenisen, Dronning Maud Land, Antarctica., Ann. Glaciol., 35, 347–354, doi:10.3189/172756402781816474, 2002.

Hamran, S.-E. and Aarholt, E.: Glacier study using wavenumber domain synthetic aperture radar, Radio Sci., 28, 559–570, doi:10.1029/92RS03022, 1993.

Hamran, S.-E., Gjessing, D. T., Hjelmstad, J., and Aarholt, E.: Ground penetrating synthetic pulse radar: Dynamic range and modes of operation, J. Appl. Geophys., 33, 7–14, doi:10.1016/0926-9851(95)90025-X, 1995.

Haran, T., Bohlander, J., Scambos, T., Painter, T., and Fahnestock, M.: MODIS mosaic of Antarctica (MOA) image map, in: National Snow and Ice Data Center, Digital media, Boulder, Colorado USA, 2005, updated 2006.

Helsen, M., Van den Broeke, M., Van de Wal, R., Van de Berg, W., Van Meijgaard, E., Davis, C., Li, Y., and Goodwin, I.: Elevation changes in Antarctica mainly determined by accumulation variability, Science, 320, 1626–1629, doi:10.1126/science.1153894, 2008.

Hirasawa, N., Nakamura, H., and Yamanouchi, T.: Abrupt changes in meteorological conditions observed at an inland Antarctic Station in association with wintertime blocking, Geophys. Res. Lett., 27, 1911–1914, doi:10.1029/1999GL011039, 2000.

Hirasawa, N.: Winter warming-event observed at Dome Fuji Station and synoptic-scale circulation in the Antarctic, Nankyoku Shiryo

(Antarctic Record), 54, 292–307, 2010.

Hofstede, C. M., Van de Wal, R. S. W., Kaspers, K. A., Van den Broeke, M. R., Karlöf, L., Winther, J.-G., Isaksson, E., Lappegard, G., Mulvaney, R., Oerter, H., and Wilhelms, F.: Firn accumulation records for the past 1000 years on the basis of dielectric profiling of six cores from Dronning Maud Land, Antarctica, J. Glaciol., 50, 279–291, doi:10.3189/172756504781830169, 2004.

Holmlund, P. and Fujita, S.: Japanese-Swedish Antarctic Expedition JASE, edited by: Thorén A., Swedish Polar Secretariat Year Book 2008, Stockholm, 18E1, 2009.

Huybrechts, P., Rybak, O., Pattyn, F., and Steinhage, D.: Past and present accumulation rate reconstruction along the Dome Fuji-Kohnen radio echo sounding profile, Dronning Maud Land, East Antarctica, Ann. Glaciol., 50, 112–120, doi:10.3189/172756409789097513, 2009.

Igarashi, M., Nakai, Y., Motizuki, Y., Takahashi, K., Motoyama, H., and Makishima, K.: Dating of the Dome Fuji shallow ice core based on a record of volcanic eruptions from AD 1260 to AD 2001, Polar Sci., 5, 411–420, doi:10.1016/j.polar.2011.08.001, 2011.

Isaksson, E., Karlén, W., Gundestrup, N., Mayewski, P., Whitlow, S., and Twickler, M.: A century of accumulation and temperature changes in Dronning Maud Land, Antarctica, J. Geophys. Res., 101, 7085–7094, doi:10.1029/95JD03232, 1996.

Isaksson, E., Van den Broeke, M. R., Winther, J.-G., Karlöf, L., Pinglot, J. F., and Gundestrup, N.: Accumulation and proxy-temperature variability in Dronning Maud Land, Antarctica, determined from shallow firn cores, Ann. Glaciol., 29, 17–22, doi:10.3189/172756499781821445, 1999.

Japan Meteorological Agency: Antarctic Meteorological Data Vol. 44, obtained by the 44th Japanese Antarctic Research Expedition at Syowa Station and Dome Fuji Station in 2003, CD-ROM, Japan Meteorological Agency, Tokyo, 2005.

Kameda, T., Motoyama, H., Fujita, S., and Takahashi, S.: Temporal and spatial variability of surface mass balance at Dome Fuji, East Antarctica, by the stake method from 1995 to 2006, J. Glaciol., 54, 107–116, doi:10.3189/002214308784409062, 2008.

Karlöf, L., Isaksson, E., Winther, J.-G., Gundestrup, N., Meijer, H. A. J., Mulvaney, R., Pourchet, M., Hofstede, C.,Lappegard, G., Pettersson, R., Van den Broeke, M., and Van de Wal, R. S. W.: Accumulation variability over a small area in East Dronning Maud Land, Antarctica, as determined from shallow firn cores and snow pits: Some implications for ice-core records, J. Glaciol., 51, 343–352, doi:10.3189/172756505781829232, 2005.

Kawamura, K., Parrenin, F., Lisiecki, L., Uemura, R., Vimeux, F., Severinghaus, J. P., Hutterli, M.A., Nakazawa, T., Aoki, S., Jouzel, J., Raymo, M.E., Matsumoto, K., Nakata, H., Motoyama, H., Fujita, S., Azuma, K., Fujii, Y. and Watanabe, O.: Northern Hemisphere forcing of climatic cycles over the past 360,000 years implied by accurately dated Antarctic ice cores, Nature, 448, 912–916, doi:10.1038/nature06015, 2007.

Keller, L. M., Lazzara, M. A., Thom, J. E., Weidner, G. A., and Stearns, C. R.: Antarctic Automatic Weather Station Data for the calendar year 2009, Space Science and Engineering Center, University of Wisconsin, Madison, Wisconsin, 2010.

Kikuchi, T.: Prevailing Windfield, in: Antarctica: East Queen Maud Land-Enderby Land Glaciological Folio, Sheet 2, National Insti-

tute of Polar Research, Tokyo, Japan, 1997.

King, J. C. and Turner, J.: Antarctic Meteorology and Climatology, 409 pp., Cambridge Univ. Press, New York, 1997.

Kovacs, A., Gow, A. J., and Morey, R. M.: The in-situ dielectric constant of polar firn revisited, Cold Reg. Sci. Technol., 23, 245–256, doi:10.1016/0165-232X(94)00016-Q, 1995.

Krinner, G., Magand, O., Simmonds, I., Genthon, C. and Dufresne, J.-L.: Simulated Antarctic precipitation and surface mass balance at the end of the twentieth and twenty-first centuries, Clim. Dyn., 28, 215–230, doi:10.1007/s00382-006-0177-x, 2007.

Legrand, M. and Wagenbach, D.: Impact of Cerro Hudson and Pinatubo volcanic eruptions on the Antarctic air and snow chemistry, J. Geophys. Res., 104, 1581–1596, doi:10.1029/1998JD100032, 1999.

Lemke, P., Ren, J., Alley, R. B., Allison, I., Carrasco, J., Flato, G., Fujii, Y., Kaser, G., Mote, P., Thomas, R. H., and Zhang, T.: Observations: Changes in Snow, Ice and Frozen Ground, in: Climate change 2007: the physical science basis. Contribution of Working Group I to the Fourth Assessment Report of the Intergovernmental Panel on Climate Change, edited by: Solomon, S., Qin, D., Manning, M., Chen, Z., Marquis, M., Averyt, K. B., Tignor, M., and Miller, H. L., Cambridge University Press, Cambridge, 2007.

Matsuoka, K., Maeno, H., Uratsuka, S., Fujita, S., Furukawa, T., and Watanabe, O.: A ground-based, multi-frequency ice-penetrating radar system, Ann. Glaciol., 34, 171–176, doi:10.3189/172756402781817400, 2002.

Monaghan, A., Bromwich, D., Fogt, R., Wang, S., Mayewski, P., Dixon, D., Ekaykin, A., Frezzotti, M., Goodwin, I., Isaksson, E., Kaspari, S., Morgan, V., Oerter, H., Van Ommen, T., Van Der Veen, C. and Wen, J..: Insignificant change in Antarctic snowfall since the International Geophysical Year, Science, 313, 827–831, doi:10.1126/science.1128243, 2006.

Motoyama, H., Enomoto, H., Furukawa, T., Kamiyama, K., Shoji, H., Shiraiwa, T., Watanabe, K., Namasu, K., and Ikeda, H.: Preliminary study of ice flow observations along traverse routes from coast to Dome Fuji, East Antarctica by differential GPS method., Nankyoku Shiryo (Antarctic Record), 39, 94–98, 1995.

Moore, J. C., Mulvaney, R., and Paren, J. G.: Dielectric stratigraphy of ice: a new technique for determining total ionic concentrations in polar ice, Geophys. Res. Lett., 16, 1177–1180, doi:10.1029/GL016i010p01177, 1989.

Mosley-Thompson, E., Paskievitch, J. F., Gow, A. J., and Thompson, L. G.: Late 20th century increase in South Pole snow accumulation, J. Geophys. Res., 104(D4), 3877–3886, doi:10.1029/1998JD200092, 1999.

Müller, K., Sinisalo, A., Anschütz, H., Hamran, S.-E., Hagen, J.-O., McConnell, J. R., and Pasteris, D. R.: An 860 km surface mass-balance profile on the East Antarctic plateau derived by GPR, Ann. Glaciol., 55, 1–8, doi:10.3189/172756410791392718, 2010.

Noone, D. and Simmonds, I.: Implications for interpretations of ice-core isotope data from analysis of modelled Antarctic precipitation, Ann. Glaciol., 27, 398–402, 1998.

Noone, D., Turner, J., and Mulvaney, R.: Atmospheric signals and characteristics of accumulation in Dronning Maud Land, Antarctica, J. Geophys. Res., 104, 19191–19211, doi:10.1029/1999JD900376, 1999.

Oerter, H., Wilhelms, F., Jung-Rothenhäusler, F., Göktas, F., Miller,

H., Graf, W., and Sommer, S.: Accumulation rates in Dronning Maud Land, Antarctica, as revealed by dielectric-profiling measurements of shallow firn cores, Ann. Glaciol., 30, 27–34, doi:10.3189/172756400781820705, 2000.

Oerter, H., Graf, W., Meyer, H., and Wilhelms, F.: The EPICA ice core from Dronning Maud Land: first results from stable-isotope measurements, Ann. Glaciol., 39, 307–312, doi:10.3189/172756404781814032, 2004.

Parrenin, F., Dreyfus, G., Durand, G., Fujita, S., Gagliardini, O., Gillet, F., Jouzel, J., Kawamura, K., Lhomme, N., Masson-Delmotte, V., Ritz, C., Schwander, J., Shoji, H., Uemura, R., Watanabe, O., and Yoshida, N.: 1-D-ice flow modelling at EPICA Dome C and Dome Fuji, East Antarctica, Clim. Past, 3, 243–259, doi:10.5194/cp-3-243-2007, 2007.

Pruett, L. E., Kreutz, K. J., Wadleigh, M., Mayewski, P. A., and Kurbatov, A.: Sulfur isotopic measurements from a West Antarctic ice core: implications for sulphate source and transport, Ann. Glaciol., 39, 161–168, doi:10.3189/172756404781814339, 2004.

Reijmer, C. and Van den Broeke, M. R.: Temporal and spatial variability of the surface mass balance in Dronning Maud Land, Antarctica, as derived from automatic weather stations, J. Glaciol., 49, 512–520, doi:10.3189/172756503781830494, 2003.

Richardson, C., Aarholt, E., Hamran, S.-E., Holmlund, P., and Isaksson, E.: Spatial distribution of snow in western Dronning Maud Land, East Antarctica, mapped by a ground-based snow radar, J. Geophys. Res., 102, 20343–20353, doi:10.1029/97JB01441, 1997.

Roe, G. H.: Orographic precipitation, Annu. Rev. Earth Planet. Sci., 33, 645–671, 2005. doi:10.1146/annurev.earth.33.092203.122541, 2005.

Rotschky, G., Eisen, O., Wilhelms, F., Nixdorf, U., and Oerter, H.: Spatial distribution of surface mass balance on Amundsenisen plateau, Antarctica, derived from ice-penetrating radar studies, Ann. Glaciol., 39, 265–270, doi:10.3189/172756404781814618, 2004.

Rotschky, G., Holmlund, P., Isaksson, E., Mulvaney, R., Oerter, H., Van den Broecke, M. R., and Winther, J.-G.: A new surface accumulation map for western Dronning Maud Land, Antarctica, from interpretation of point measurements, J. Glaciol., 53, 385–398, doi:10.3189/002214307783258459, 2007.

Ruth, U., Barnola, J.-M., Beer, J., Bigler, M., Blunier, T., Castellano, E., Fischer, H., Fundel, F., Huybrechts, P., Kaufmann, P., Kipfstuhl, S., Lambrecht, A., Morganti, A., Oerter, H., Parrenin, F., Rybak, O., Severi, M., Udisti, R., Wilhelms, F., and Wolff, E.: "EDML1": a chronology for the EPICA deep ice core from Dronning Maud Land, Antarctica, over the last 150 000 years, Clim. Past, 3, 475–484, doi:10.5194/cp-3-475-2007, 2007.

Schlosser, E., Duda, M. G., Powers, J. G., and Manning, K. W.: Precipitation regime of Dronning Maud Land, Antarctica, derived from Antarctic Mesoscale Prediction System (AMPS) archive data, J. Geophys. Res., 113, D24108, doi:10.1029/2008JD009968, 2008.

Schlosser, E., Manning, K.W., Powers, J.G., Duda, M.G., Birnbaum, G., and Fujita, K.: Characteristics of high precipitation events in Dronning Maud Land, Antarctica, J. Geophys. Res, 115, D14107, doi:10.1029/2009JD013410, 2010.

Stenni, B., Proposito, M., Gragnani, R., Flora, O., Jouzel, J.,

Falourd, S., and Frezzotti, M.: Eight centuries of volcanic signal and climate change at Talos Dome (East Antarctica), J. Geophys. Res., 107, 4076, doi:10.1029/2000JD000317, 2002.

Surdyk, S.: Using microwave brightness temperature to detect short-term surface air temperature changes in Antarctica: An analytical approach, Remote Sens. Environ., 80, 256–271, doi:10.1016/S0034-4257(01)00308-X, 2002.

Surdyk, S. and Fily, M.: Comparison of the passive microwave spectral signature of the Antarctic ice sheet with ground traverse data, Ann. Glaciol., 17, 161–166, 1993.

Surdyk, S. and Fily, M.: Results of a stratified snow emissivity model based on the wave approach: Application to the Antarctic Ice Sheet, J. Geophys. Res., 100, 8837–8848, doi:10.1029/94JC03361, 1995.

Takahashi, S., Kameda, T., Enomoto, H., Motoyama, H., and Watanabe, O.: Automatic Weather Station (AWS) data collected by the 33rd to 42nd Japanese Antarctic Research Expeditions during 1993–2001 in: JARE data reports, Meteorology, National Institute of Polar Research, Tokyo, 416 pp., 2004.

Trauffetter, F., Oerter, H., Fischer, H., Weller, R., and Miller, H.: Spatio-temporal variability in volcanic sulphate deposition over the past 2 kyr in snow pits and firn cores from Amundsenisen, Dronning Maud Land, Antarctica, J. Glaciol., 50, 137–146, doi:10.3189/172756504781830222, 2004

Urbini, S., Frezzotti, M., Gandolfi, S., Vincent, C., Scarchilli, C., Vittuari, V., and Fily, M.: Historical behaviour of Dome C and Talos Dome (East Antarctica) as investigated by snow accumulation and ice velocity measurements, Global Planet. Change, 60, 576–588, doi:10.1016/j.gloplacha.2007.08.002, 2008.

Van de Berg, W., Van den Broeke, M., Reijmer, C., and Van Meijgaard, E.: Reassessment of the Antarctic surface mass balance using calibrated output of a regional atmospheric climate model, J. Geophys. Res., 111, D11104, doi:10.1029/2005JD006495, 2006.

Van As, M. R., Van den Broeke, M. R., and Helsen, M.: Strong-wind events and their impact on the near-surface climate at Kohnen Station on the Antarctic Plateau, Antarct. Sci., 19, 507–519, doi:10.1017/S095410200700065X, 2007.

Van den Broeke, M. R. and Van Lipzig, N. P. M.: Factors controlling the near-surface wind field in Antarctica, Mon. Weather Rev., 131, 733–743, doi:10.1175/1520-0493(2003)131<0733:FCTNSW>2.0.CO;2, 2003.

Van Lipzig, N. P. M., Turner, J., Colwell, S. R., and Van den Broeke, M. R.: The near-surface wind field over the Antarctic continent, Int. J. Climatol., 24, 1973–1982, doi:10.1002/joc.1090, 2004.

Vaughan, D., Bamber, J., Giovinetto, M., Russell, J., and Cooper, A.: Reassessment of net surface mass balance in Antarctica, J. Climate, 45, 933–946, doi:10.1175/1520-0442(1999)012<0933:RONSMB>2.0.CO;2, 1999.

Velicogna, I. and Wahr, J.: Measurements of time-variable gravity show mass loss in Antarctica, Science, 311, 1754–1756, doi:10.1126/science.1123785, 2006.

Watanabe, O.: Distributions of surface features of snow cover in Mizuho Plateau., Mem. Natl Inst. Polar Res. Spec. Issue., 7, 44–62, 1978.

Watanabe, O., Fujii, Y., Motoyama, H., Furukawa, T., Shoji, H., Enomoto, H., Kameda, T., Narita, H., Naruse, R., Hondoh, T., Fujita, S., Mae, S., Azuma, N., Kobayashi, S., Nakawo, M., and Ageta, Y.: Preliminary study of ice core chronology at Dome

Fuji, Proc. NIPR Symp. Polar Meteorol. Glaciol., 11, 9–13, 1997.

Watanabe, O., Jouzel, J., Johnsen, S., Parrenin, F., Shoji, H., and Yoshida, N.: Homogeneous climate variability across East Antarctica over the past three glacial cycles, Nature, 422, 509–512, doi:10.1038/nature01525, 2003.

Wilhelms, F.: Explaining the dielectric properties of firn as a density-and-conductivity mixed permittivity (DECOMP), Geophys. Res. Lett., 32, L16501, doi:10.1029/2005GL022808, 2005.

Wilhelms, F., Kipfstuhl, J., Miller, H., Heinloth, K., and Firestone, J.: Precise dielectric profiling of ice cores: a new device with improved guarding and its theory, J. Glaciol., 44, 171–174, 1998.